Exact two-component Hamiltonians for relativistic quantum chemistry

Stefan Knecht, Michal Repisky, Hans Jørgen Aagaard Jensen, Trond Saue

Exact two-component Hamiltonians for relativistic quantum chemistry: Two-electron picture-change corrections made simple

Stefan Knecht,[1,2,3,a)] Michal Repisky,[4,b)] Hans Jørgen Aagaard Jensen,[5] and Trond Saue[6]
[1)] *Algorithmiq Ltd, Kanavakatu 3C, FI-00160 Helsinki, Finland*
[2)] *SHE Chemie, GSI Helmholtzzentrum für Schwerionenforschung GmbH, Planckstr. 1, 64291 Darmstadt, Germany*
[3)] *Department of Chemistry, Johannes-Gutenberg Universität Mainz, Duesbergweg 10-14, 55128 Mainz, Germany*
[4)] *Hylleraas Centre for Quantum Molecular Sciences, Department of Chemistry, UiT–The Arctic University of Norway, N-9037 Tromsø, Norway*
[5)] *Department of Physics, Chemistry and Pharmacy, University of Southern Denmark, Campusvej 55, DK-5230 Odense M, Denmark*
[6)] *Laboratoire de Chimie et Physique Quantiques (CNRS UMR 5626), Université Toulouse III – Paul Sabatier, 118 Route de Narbonne, F-31062 Toulouse cedex, France*

(Dated: October 28, 2022)

Based on self-consistent field (SCF) atomic mean-field (amf) quantities, we present two simple, yet computationally efficient and numerically accurate matrix-algebraic approaches to correct both scalar-relativistic *and* spin-orbit two-electron picture-change effects (PCE) arising within an exact two-component (X2C) Hamiltonian framework. Both approaches, dubbed amfX2C and e(xtended)amfX2C, allow us to uniquely tailor PCE corrections to mean-field models, *viz.* Hartree–Fock or Kohn–Sham DFT, in the latter case also avoiding the need of a point-wise calculation of exchange–correlation PCE corrections. We assess the numerical performance of these PCE correction models on spinor energies of group-18 (closed-shell) and group-16 (open-shell) diatomic molecules, achieving a consistent $\approx 10^{-5}$ Hartree accuracy compared to reference four-component data. Additional tests include SCF calculations of molecular properties such as absolute contact density and contact density shifts in copernicium fluoride compounds (CnF_n, n=2,4,6), as well as equation-of-motion coupled cluster calculations of X-ray core ionization energies of 5*d* and 6*d*-containing molecules, where we observe an excellent agreement with reference data. To conclude, we are confident that our (e)amfX2C PCE correction models constitute a fundamental milestone towards a universal and reliable relativistic two-component quantum chemical approach, maintaining the accuracy of the parent four-component one at a fraction of its computational cost.

I. INTRODUCTION

Advancing with rapid strides in the past decades, relativistic quantum chemical approaches are becoming a standard ingredient in the computational toolbox of theoretical chemists. Notwithstanding important steps forward to turn a fully relativistic quantum-chemical approach based on the four-component Dirac formalism into a handy tool[1–9], much of the success is due to the fast-paced development and implementation of efficient quasi-relativistic "exact" two-component approaches (X2C)[10] in various originally non-relativistic popular quantum-chemistry software packages within the past two decades. This has become possible by making use of a matrix-algebra formalism rather than setting out from an (order-by-order) based operator formalism[11–19].

In relativistic quantum chemistry, the common starting point for almost all of the matrix-algebra-based two-component (2c) Hamiltonian approaches, whether formulated within an elimination ansatz[20–23] or in a unitary-decoupling framework,[24–30] has been the four-component (4c) *one-electron* Dirac Hamiltonian in the electrostatic potential of fixed nuclei.[3] We will in the following refer to the 4c Hamiltonian used to construct a 2c model as the *defining* 4c Hamiltonian. In the case of the one-electron X2C Hamiltonian scheme (1eX2C), the two-electron (2e) interaction term is omitted from the defining 4c Dirac Hamiltonian. Consequently, the resulting 2c Hamiltonian is to be considered "exact" only wrt the inclusion of 1e terms in the defining 4c Hamiltonian[31], while the account of the 2e interaction is postponed to *after* having carried out the unitary decoupling of the 1e Hamiltonian and the ensuing restriction to the upper ("electrons-only") 2c spinor basis. Such an approach usually implies the use of the *untransformed* 2e interaction term in the 1eX2C basis set, giving rise to 2e picture-change effects (2ePCEs). A

[a)] Electronic mail: stefan@algorithmiq.fi
[b)] Electronic mail: michal.repisky@uit.no

noticeable exception exists, though, and has been coined the molecular–mean field exact two-component approach (mmfX2C).[32] In contrast to the 1eX2C scheme, the mmfX2C *ansatz* is based on a unitary decoupling of the 4c molecular mean-field *Fock matrix* after having converged the 4c self-consistent field (SCF) Hartree–Fock equations. Although strictly matching with the SCF results of those obtained with the corresponding defining 4c Hamiltonian,[27,32] the mmfX2C approach will still be an approximation in any ensuing post-SCF electron-correlation step for which the untransformed 2e interaction term replaces its complete (transformed) counterpart.

Hence, the extent to which 2ePCEs are accounted for in an X2C Hamiltonian based relativistic quantum-chemical framework is essential for its applicability to address the electronic-structure theory problem in many-electron (molecular) systems involving elements across the entire periodic table.[31] To this end, we note that the 2e interaction term can be decomposed into a spin-free or scalar-relativistic (SC) as well as a spin-dependent or spin-orbit (SO) part,[1,33] where both the two-electron scalar-relativistic (2eSC) and two-electron spin-orbit (2eSO) terms serve as a screening of their 1e counterparts. Whereas much attention has been paid in the past to efficiently take into account 2eSO PCEs based on a variety of *ansätze*, the 2eSC contributions are, curiously, less commonly included in correction schemes for 2ePCEs as has been comprehensively summarized in the Introduction of Ref. 34. Examples of approximate 2eSO corrections range from using (i) a parametrized model approach based on nuclear charges multiplied with element and angular-momentum specific screening factors in the evaluation of 1eSO integrals;[35,36] (ii) a mean-field SO approach[37] which has been the basis for the widely popular AMFI module[38] interfaced for example with the software packages DIRAC,[5] OpenMolcas,[39], and DALTON;[40] (iii) an approach that exploits atomic model densities obtained within the framework of Kohn–Sham DFT (KS-DFT).[41–43] Interestingly, although the latter model-density based correction schemes are rare examples which in addition to corrections for 2eSO PCEs do provide corrections for 2eSC PCEs, the resulting correction terms do not discriminate between the use of different exchange-correlation functionals employed in a *molecular* X2C-Hamiltonian based Kohn-Sham DFT calculation. The screening factors of type (i) are sometimes referred to as "Boettger factors" or as the screened–nuclear–spin–orbit (SNSO) approach.[44] In current usage they have been obtained for a second-order, truncated 2c Hamiltonian *ansatz* (i.e. second-order Douglas–Kroll–Hess (DKH2)) within the framework of density functional theory (DFT)[44] but are, remarkably, also commonly employed in X2C-Hamiltonian based wave function theory (WFT) approaches[45–47] To overcome this discrepancy for their use in exact two-component theories, the original SNSO approach has been reparametrized based on atomic four-component Dirac-Hartree-Fock results.[48] The resulting *modified* SNSO approach led to a further improvement for the calculation of molecular properties in a two-component framework with respect to the parent four-component results.[48,49]

In their most recent work on suitable 2ePCE corrections for the X2C Hamiltonian, Liu and Cheng[34] proposed an atomic mean-field (amf) approach which exploits a mean-field approximation for PCEs originating from the 2eSO contribution, dubbed SOX2CAMF by them, and combines "the four main ideas in relativistic quantum chemistry (...): the X2C decoupling scheme, the 1e approximation for SC effects (i.e., the neglect of the scalar 2e picture-change effects), the mean-field SO approach, and the atomic approximation for the 2eSO interactions".[34] Thus, a key feature of the SOX2CAMF model is that it does not require the evaluation of any *molecular* relativistic 2e integrals. Although it has in the meantime been employed successfully in highly sophisticated electron correlation calculations of heavy-element complexes,[50] limitations of the underlying atomic approximation to account for 2eSO PCEs have recently been pointed out in the context of zero-field splittings of first-row transition metal complexes.[51]

In this paper we introduce an atomic mean-field (amfX2C) as well as an extended atomic mean-field (eamfX2C) approach within the X2C Hamiltonian framework which not only takes into account the above mentioned four main ideas in relativistic quantum chemistry but also amends them such that the resulting amfX2C and eamfX2C approaches will bridge the gap between a full molecular 4c and mmfX2C framework in a computationally efficient, yet highly accurate way. In contrast to most existing correction schemes for 2ePCE, our amfX2C and eamfX2C approaches are laid out to comprise *full* 2ePCE corrections, that is treating the 2eSO *and* 2eSC ones on the same footing, whether they arise from the (relativistic) 2e Coulomb, Coulomb-Gaunt, or Coulomb-Breit interaction. Moreover, our *ansatz* takes into account the characteristics of the underlying correlation framework, *viz.*, WFT or (KS-)DFT, which enables us to introduce tailor-made exchange-correlation-specific corrections for 2ePCEs. Setting out from the idea of an amf approach within the amfX2C Hamiltonian model – formulated for a WFT-based HF and a DFT framework in Sections II A and II B, respectively – the *extended* amfX2C approach encompasses two-center 2e contributions obtained in a molecular framework. The implications arising from the resulting eamfX2C approach, including its potential shortcomings and particular advantages are then discussed in Section II C. The numerical accuracy of both (e)amfX2C Hamiltonian models are assessed based on the calculation of a variety of valence and core-like molecular properties in Section IV where the computational details are given in Section III. We summarize our results and findings in Section V and provide a prospect of future developments.

II. THEORY

A. The amfX2C Hamiltonian – Hartree–Fock framework

A convenient starting point for our derivations to arrive at suitable corrections for 2ePCEs in an X2C Hamiltonian framework is to consider the closed-shell 4c HF equations based on the Dirac–Coulomb Hamiltonian

$$\boldsymbol{F}^{4c}\boldsymbol{c}_i^{4c} = \boldsymbol{c}_i^{4c}\epsilon_i^{4c}. \tag{1}$$

For convenience (see below), we express these equations in the orthonormal basis obtained from the initial AO-basis by some suitable orthogonalization procedure.[52] The HF energy and the Fock matrix have their usual definitions

$$E^{4c} = E^{4c,1e} + E^{4c,2e} = \sum_{\mu\nu} h^{4c}_{\mu\nu} D^{4c}_{\nu\mu} + \frac{1}{2}\sum_{\mu\nu\kappa\lambda} D^{4c}_{\nu\mu} G^{4c}_{\mu\nu,\kappa\lambda} D^{4c}_{\lambda\kappa} \tag{2}$$

$$F^{4c}_{\mu\nu} = F^{4c,1e}_{\mu\nu} + F^{4c,2e}_{\mu\nu} = h^{4c}_{\mu\nu} + \sum_{\kappa\lambda} G^{4c}_{\mu\nu,\kappa\lambda} D^{4c}_{\lambda\kappa} = \frac{\mathrm{d}E^{4c}}{\mathrm{d}D^{4c}_{\nu\mu}} \tag{3}$$

in terms of the atomic orbital (AO) density matrix

$$D^{4c}_{\mu\nu} = \sum_i^{\mathrm{occ}} c^{4c}_{\mu i} c^{4c^*}_{\nu i} \tag{4}$$

and the matrix of anti-symmetrized two-electron AO integrals

$$G^{4c}_{\mu\nu,\kappa\lambda} = \mathcal{I}^{4c}_{\mu\nu,\kappa\lambda} - \mathcal{I}^{4c}_{\mu\lambda,\kappa\nu}; \quad \mathcal{I}^{4c}_{\mu\nu,\kappa\lambda} \equiv \iint \Omega^{4c}_{\mu\nu}(\boldsymbol{r}_1) r_{12}^{-1} \Omega^{4c}_{\kappa\lambda}(\boldsymbol{r}_2) d^3\boldsymbol{r}_1 d^3\boldsymbol{r}_2, \tag{5}$$

the latter expressed in terms of overlap distribution functions[6]

$$\Omega^{4c}_{\mu\nu}(\boldsymbol{r}) \equiv \int \chi^\dagger_\mu(\boldsymbol{r}')\delta^3(\boldsymbol{r}'-\boldsymbol{r})\chi_\nu(\boldsymbol{r}')d^3\boldsymbol{r}' = \chi^\dagger_\mu(\boldsymbol{r})\chi_\nu(\boldsymbol{r}) \tag{6}$$

over 2-component basis functions $\chi_\mu(\boldsymbol{r})$; formally the basis functions are 4-component objects, but with the lower or upper two components zero according to whether they are large (L) or small (S).

The *converged* HF equations, Eq. (1), form the starting point for the mmfX2C approach,[32] where the Fock matrix and corresponding positive-energy molecular-orbital (MO) coefficients (+) are picture-changed to 2c form. Our computer implementations[28,30] generate the picture-change transformation matrix $\boldsymbol{U}$ in orthonormal basis since this provides control on possible linear dependencies and simplifies the construction of the appropriate metric.[29] The picture-change matrix is subsequently transformed back to the initial AO-basis. For simplicity, and without loss of generality, we shall consider the PC-transformation in orthonormal basis. Starting from Eq. (1) we therefore write

$$\tilde{F}^{2c}_{\mu\nu} \equiv \left[\boldsymbol{U}^\dagger \boldsymbol{F}^{4c} \boldsymbol{U}\right]^{\mathrm{LL}}_{\mu\nu}; \qquad \tilde{c}^{2c}_{\mu i} \equiv \left[\boldsymbol{U}^\dagger \boldsymbol{c}^{4c}\right]^{\mathrm{L+}}_{\mu i} \tag{7}$$

(note that we use tildes to indicate picture-change transformed quantities). These quantities, together with the anti-symmetrized two-electron AO integrals, Eq. (5), are then used to build the normal-ordered Hamiltonian for use in subsequent wave-function based correlation methods.

In the present case we rather seek to carry out the SCF-iterations themselves in 2c mode, but in a manner such that we optimally reproduce the 4c results. A first important observation comes from consideration of the picture-change transformed Fock matrix

$$\tilde{F}^{2c}_{\mu\nu} = \sum_{XY}\sum_{\alpha\beta} \left[U^\dagger\right]^{\mathrm{LX}}_{\mu\alpha} \left[F^{4c}\right]^{\mathrm{XY}}_{\alpha\beta} \left[U\right]^{\mathrm{YL}}_{\beta\nu}; \quad \mathrm{X,Y} \in \mathrm{L,\,S} \tag{8}$$

Noting that the positive-energy 4c MO-coefficients can be expressed in terms of their 2c counterparts

$$\boldsymbol{c}^{4c;+} = \boldsymbol{U}\tilde{\boldsymbol{c}}^{2c} \qquad \Rightarrow \qquad \left[c^{4c}\right]^{\mathrm{X+}}_{\mu i} = \sum_\nu \left[U\right]^{\mathrm{XL}}_{\mu\nu} \left[\tilde{c}^{2c}\right]_{\nu i}; \qquad \mathrm{X} \in \mathrm{L,\,S}, \tag{9}$$

we can reformulate the two-electron 2c Fock matrix as

$$\tilde{F}^{2c,2e}_{\mu\nu} = \sum_{XY}\sum_{\alpha\beta}\left[U^\dagger\right]^{LX}_{\mu\alpha}\left[F^{4c,2e}\right]^{XY}_{\alpha\beta}\left[U\right]^{YL}_{\beta\nu} \tag{10}$$

$$= \sum_{XY}\sum_{\alpha\beta}\left[U^\dagger\right]^{LX}_{\mu\alpha}\left\{\sum_{UV}\sum_{\gamma\delta}\left[G^{4c}\right]^{XY,UV}_{\alpha\beta,\gamma\delta}\left[D^{4c}\right]^{VU}_{\delta\gamma}\right\}\left[U\right]^{YL}_{\beta\nu}$$

$$= \sum_{XY}\sum_{\alpha\beta}\left[U^\dagger\right]^{LX}_{\mu\alpha}\left\{\sum_{UV}\sum_{\gamma\delta}\left[G^{4c}\right]^{XY,UV}_{\alpha\beta,\gamma\delta}\sum_{\kappa\lambda}\sum_{i}\left[U\right]^{VL}_{\delta\kappa}\left[\tilde{c}^{2c}\right]_{\kappa i}\left[\tilde{c}^{2c^*}\right]_{\lambda i}\left[U^*\right]^{UL}_{\gamma\lambda}\right\}\left[U\right]^{YL}_{\beta\nu}$$

$$= \sum_{\kappa\lambda}\left\{\sum_{XYUV}\sum_{\alpha\beta\gamma\delta}\left[U^\dagger\right]^{LX}_{\mu\alpha}\left[U^\dagger\right]^{LU}_{\lambda\gamma}\left[G^{4c}\right]^{XY,UV}_{\alpha\beta,\gamma\delta}\left[U\right]^{VL}_{\delta\kappa}\left[U\right]^{YL}_{\beta\nu}\right\}\left[\tilde{D}^{2c}\right]_{\kappa\lambda}; \qquad \text{X,Y,U,V} \in \text{L, S.} \tag{11}$$

As a consequence

$$\tilde{F}^{2c}_{\mu\nu} = \tilde{h}^{2c}_{\mu\nu} + \sum_{\kappa\lambda}\tilde{G}^{2c}_{\mu\nu,\kappa\lambda}\tilde{D}^{2c}_{\lambda\kappa}. \tag{12}$$

We see that the picture-change transformed Fock matrix can be expressed in terms of the picture-changed transformed coefficients as well as the picture-changed one- and two-electron integrals. By similar manipulations we can also show that the 4c HF energy can be expressed in terms of corresponding 2c quantities, that is

$$E^{4c} = \sum_{XY}\sum_{\mu\nu}\left[h^{4c}\right]^{XY}_{\mu\nu}\left[D^{4c}\right]^{YX}_{\nu\mu} + \frac{1}{2}\sum_{XYUV}\sum_{\mu\nu\kappa\lambda}\left[D^{4c}\right]^{YX}_{\nu\mu}\left[G^{4c}\right]^{XYUV}_{\mu\nu,\kappa\lambda}\left[D^{4c}\right]^{VU}_{\lambda\kappa}$$

$$= \sum_{\mu\nu}\left[\tilde{h}^{2c}\right]_{\mu\nu}\left[\tilde{D}^{2c}\right]_{\nu\mu} + \frac{1}{2}\sum_{\mu\nu\kappa\lambda}\left[\tilde{D}^{2c}\right]_{\nu\mu}\left[\tilde{G}^{2c}\right]_{\mu\nu,\kappa\lambda}\left[\tilde{D}^{2c}\right]_{\lambda\kappa} = \tilde{E}^{2c,1e} + \tilde{E}^{2c,2e}. \tag{13}$$

We conclude that provided we start from the *correctly transformed* set of integrals the 2c SCF will converge to the coefficients $\left\{\tilde{\boldsymbol{c}}^{2c}_i\right\}$ corresponding to the converged 4c SCF and we shall furthermore reproduce the positive orbital energies as well as total energy of the parent 4c HF. However, the picture-change transformation $\boldsymbol{U}$ associated with the converged 4c Fock matrix is *not* available at the start of the SCF-iterations, forcing us to introduce approximations.

With this in view, a second important observation arises from comparison of Eq. (12) with the Fock matrix built with *untransformed* two-electron integrals $G^{2c}_{\mu\nu,\kappa\lambda}$

$$F^{2c}_{\mu\nu} = \tilde{h}^{2c}_{\mu\nu} + \sum_{\kappa\lambda}G^{2c}_{\mu\nu,\kappa\lambda}\tilde{D}^{2c}_{\lambda\kappa}. \tag{14}$$

We immediately find that their difference expresses the picture-change correction of the two-electron integrals

$$\Delta\tilde{F}^{2c}_{\mu\nu} = \tilde{F}^{2c}_{\mu\nu} - F^{2c}_{\mu\nu} = \sum_{\kappa\lambda}\Delta\tilde{G}^{2c}_{\mu\nu,\kappa\lambda}\tilde{D}^{2c}_{\lambda\kappa}; \qquad \Delta\tilde{G}^{2c}_{\mu\nu,\kappa\lambda} = \tilde{G}^{2c}_{\mu\nu,\kappa\lambda} - G^{2c}_{\mu\nu,\kappa\lambda}. \tag{15}$$

Moreover, this differential Fock matrix may be used to correct the two-electron HF energy

$$\tilde{E}^{2c,2e} = \frac{1}{2}\sum_{\mu\nu\kappa\lambda}\tilde{D}^{2c}_{\nu\mu}\tilde{G}^{2c}_{\mu\nu,\kappa\lambda}\tilde{D}^{2c}_{\lambda\kappa} = \frac{1}{2}\sum_{\mu\nu}\tilde{D}^{2c}_{\nu\mu}\underbrace{\sum_{\kappa\lambda}G^{2c}_{\mu\nu,\kappa\lambda}\tilde{D}^{2c}_{\lambda\kappa}}_{F^{2c,2e}_{\mu\nu}} + \frac{1}{2}\sum_{\mu\nu}\tilde{D}^{2c}_{\nu\mu}\underbrace{\sum_{\kappa\lambda}\Delta\tilde{G}^{2c}_{\mu\nu,\kappa\lambda}\tilde{D}^{2c}_{\lambda\kappa}}_{\Delta\tilde{F}^{2c,2e}_{\mu\nu}}. \tag{16}$$

We now seek a suitable approximation for the differential two-electron Fock matrix $\Delta\tilde{\boldsymbol{F}}^{2c,2e}$. In line with previous authors we exploit the expected local atomic nature of the two-electron picture-change corrections, but we will impose the condition that the scheme should reproduce *atomic* 4c SCF calculations *exactly* at the 2c level. We accordingly start from a superposition of converged atomic quantities rather than the converged molecular one, *i.e.*

$$\Delta\tilde{\boldsymbol{F}}^{2c,2e} \simeq \Delta\tilde{\boldsymbol{F}}^{2c,2e}_{\oplus} = \bigoplus_{K=1}^{M}\Delta\tilde{\boldsymbol{F}}^{2c}_{K}[\tilde{\boldsymbol{D}}^{2c}_{K}], \tag{17}$$

where K runs over all atoms in an M-atomic system. Such an approach defines our *atomic mean-field exact two-component* scheme, denoted as amfX2C. We emphasize that the picture-change correction Eq. (17) should be expressed in the original AO-basis rather than the orthonormal one in order to avoid mixing of basis functions from different centers. However, in order to avoid notational overload we do not distinguish matrix quantities in the two different bases.

Due to the atomic nature of amfX2C two-electron picture-change corrections, their evaluation scales linearly with the system size (or sub-linearly if there are multiple instances of an atomic type). To summarize the essentials, we propose the following computational scheme to arrive at the amfX2C model:

1. For each atomic type K we perform a 4c Kramers-restricted (KR) average-of-configuration (AOC) HF calculation[53] – or, if the latter is not available, – a 4c KR fractional occupation HF calculation.
2. The converged atomic Fock matrix $\boldsymbol{F}_K^{4c}$ is exactly block-diagonalized to give its 2c counterpart $\tilde{\boldsymbol{F}}_K^{2c}$ as well as picture-changed coefficients $\tilde{\boldsymbol{c}}_K^{2c}$ and density matrix $\tilde{\boldsymbol{D}}_K^{2c}$.
3. Using the latter quantity, we build the atomic 2c Fock matrix $\boldsymbol{F}_K^{2c}[\tilde{\boldsymbol{D}}_K^{2c}]$ with untransformed two-electron integrals, Eq. (14).
4. The differential atomic Fock matrix $\Delta\tilde{\boldsymbol{F}}_K^{2c}[\tilde{\boldsymbol{D}}_K^{2c}]$ is now built according to Eq. (15).
5. The atomic matrices $\Delta\tilde{\boldsymbol{F}}_K^{2c}$ and $\boldsymbol{F}_K^{4c,2e}$ are then inserted in the appropriate atomic blocks to form approximate molecular two-electron picture-change correction matrix ($\Delta\tilde{\boldsymbol{F}}_{\oplus}^{2c,2e}$), Eq. (17), and approximate molecular two-electron Fock matrix ($\boldsymbol{F}_{\oplus}^{4c,2e}$), respectively:

$$\boldsymbol{F}^{4c,2e} \simeq \boldsymbol{F}_{\oplus}^{4c,2e} = \bigoplus_{K=1}^{M} \boldsymbol{F}_K^{4c,2e}[\boldsymbol{D}_K^{4c}]. \tag{18}$$

6. The molecular X2C decoupling matrix $\boldsymbol{U}$ is built from $\boldsymbol{h}^{4c} + \boldsymbol{F}_{\oplus}^{4c,2e}$.
7. Finally, SCF iterations are carried out with amfX2C expressions that approximate the exact molecular Fock matrix and energy expressions

$$\tilde{F}_{\mu\nu}^{2c} \simeq \tilde{F}_{\mu\nu}^{\mathrm{amfX2C}} = \underbrace{\tilde{h}_{\mu\nu}^{2c} + \Delta\tilde{F}_{\oplus,\mu\nu}^{2c,2e}}_{\text{static term}} + \underbrace{F_{\mu\nu}^{2c,2e}[\tilde{\boldsymbol{D}}^{2c}]}_{\text{dynamic term}} \tag{19}$$

$$\tilde{E}^{2c} \simeq \tilde{E}^{\mathrm{amfX2C}} = \sum_{\mu\nu} \tilde{D}_{\nu\mu}^{2c}\Big(\tilde{h}_{\mu\nu}^{2c} + \frac{1}{2}\Delta\tilde{F}_{\oplus,\mu\nu}^{2c,2e} + \frac{1}{2}F_{\mu\nu}^{2c,2e}[\tilde{\boldsymbol{D}}^{2c}]\Big). \tag{20}$$

A pseudo-code describing the essential steps of our amfX2C approach for both HF and Kohn–Sham DFT theory is listed in Alg. 1.

B. The amfX2C Hamiltonian – Kohn–Sham DFT framework

Section II A has so far exclusively focused on a discussion of 2ePCE corrections within a mean-field HF scheme. As indicated in Algorithm 1, the proposed amfX2C scheme has also the appealing feature that it can straightforwardly be extended to a KS-DFT framework.

1. The closed-shell case

We first consider the closed-shell molecular case and again start from Eq. (1), but with the Fock matrix replaced by the KS one. The 4c energy and KS matrix read

$$E^{4c} = \sum_{\mu\nu} h_{\mu\nu}^{4c} D_{\nu\mu}^{4c} + \frac{1}{2}\sum_{\mu\nu\kappa\lambda} D_{\nu\mu}^{4c} G_{\mu\nu,\kappa\lambda}^{\omega;4c} D_{\lambda\kappa}^{4c} + E_{xc}^{4c}\left[n^{4c}\right] \tag{21}$$

$$F_{\mu\nu}^{4c} = h_{\mu\nu}^{4c} + \sum_{\kappa\lambda} G_{\mu\nu,\kappa\lambda}^{\omega;4c} D_{\lambda\kappa}^{4c} + \int v_{xc}\left[n^{4c}\right](\boldsymbol{r})\,\Omega_{\mu\nu}^{4c}(\boldsymbol{r})\,d^3\boldsymbol{r}; \quad v_{xc}[n](\boldsymbol{r}) = \frac{\delta E_{xc}}{\delta n(\boldsymbol{r})}. \tag{22}$$

Here, we have generalized the anti-symmetrized two-electron AO integrals of Eq. (5) to include the weight ω of exact exchange. As usual, E_{xc} and v_{xc} refer to the exchange–correlation energy functional and the corresponding potential, respectively.

Formally E_{xc} may be expressed as an integral over an xc energy density ε_{xc}

$$E_{xc}[n] = \int \varepsilon_{xc}\left[n\right](\boldsymbol{r})\, d^3\boldsymbol{r}, \tag{23}$$

which is itself a functional of the number density (n). This allows for instance the electron number to be known locally such that the derivative discontinuity can be obeyed.[54] Crucial for the following, though, is that density functional approximations (DFA) employ *local ansätze*. For instance, on the second rung of the "Jacob's ladder" of DFA[55,56] we find the generalized gradient approximation (GGA)

$$E_{xc}[n] = \int \varepsilon_{xc}^{\mathrm{GGA}}\left(n(\boldsymbol{r}), g(\boldsymbol{r})\right) d^3\boldsymbol{r}; \quad g(\boldsymbol{r}) = \nabla n(\boldsymbol{r}) \cdot \nabla n(\boldsymbol{r}), \tag{24}$$

where each integration point just needs local input.

Proceeding at the GGA/hybrid level, we find that the picture-changed KS matrix can be expressed as

$$\tilde{F}^{2c}_{\mu\nu} = \tilde{h}^{2c}_{\mu\nu} + \sum_{\kappa\lambda} \tilde{G}^{\omega;2c}_{\mu\nu,\kappa\lambda} \tilde{D}^{2c}_{\lambda\kappa} + \int v_{xc}^{\mathrm{GGA}}\left(n^{4c}(\boldsymbol{r}), g^{4c}(\boldsymbol{r})\right) \tilde{\Omega}^{2c}_{\mu\nu}(\boldsymbol{r})\, d^3\boldsymbol{r}. \tag{25}$$

We again recover an expression in terms of picture-changed quantities, but the xc potential is seen to still use 4c variables as input. However, proceeding as in the HF case (c.f. Eq.(13) in Section II A), the number density can be re-expressed in terms of 2c quantities

$$n^{4c}(\boldsymbol{r}) = \sum_{XY}\sum_{\mu\nu} \left[\Omega^{4c}(\boldsymbol{r})\right]^{XY}_{\mu\nu} \left[D^{4c}\right]^{YX}_{\nu\mu} = \sum_{\mu\nu} \left[\tilde{\Omega}^{2c}(\boldsymbol{r})\right]_{\mu\nu} \left[\tilde{D}^{2c}\right]_{\nu\mu} = \tilde{n}^{2c}(\boldsymbol{r}). \tag{26}$$

Since the (correctly!) picture-changed transformed 2c number density $\tilde{n}^{2c}$ is identical to the parent 4c quantity at all points in space, this equivalence will also hold for their gradients, which allows us to write

$$g^{4c}(\boldsymbol{r}) = \nabla\tilde{n}^{2c}(\boldsymbol{r}) \cdot \nabla\tilde{n}^{2c}(\boldsymbol{r}) = \tilde{g}^{2c}(\boldsymbol{r}). \tag{27}$$

This also means that the xc energy and potential can be expressed entirely in terms of 2c quantities

$$\tilde{E}^{2c}_{xc} = \int \varepsilon_{xc}^{\mathrm{GGA}}\left(\tilde{n}^{2c}(\boldsymbol{r}), \tilde{g}^{2c}(\boldsymbol{r})\right) d^3\boldsymbol{r}, \tag{28}$$

$$\tilde{F}^{2c,xc}_{\mu\nu} = \int v_{xc}^{\mathrm{GGA}}\left(\tilde{n}^{2c}(\boldsymbol{r}), \tilde{g}^{2c}(\boldsymbol{r})\right) \tilde{\Omega}^{2c}_{\mu\nu}(\boldsymbol{r})\, d^3\boldsymbol{r}. \tag{29}$$

In passing we note that the direct use of the GGA xc potential leads to contributions of the form

$$F^{xc}_{\mu\nu} = \int v_{xc}^{\mathrm{GGA}}(\boldsymbol{r})\, \Omega_{\mu\nu}(\boldsymbol{r})\, d^3\boldsymbol{r}; \quad v_{xc}^{\mathrm{GGA}}(\boldsymbol{r}) = \left[\frac{\partial\varepsilon_{xc}^{\mathrm{GGA}}}{\partial n} - 2\boldsymbol{\nabla}\cdot\left(\left(\frac{\partial\varepsilon_{xc}^{\mathrm{GGA}}}{\partial g}\right)\boldsymbol{\nabla}n\right)\right](\boldsymbol{r}). \tag{30}$$

However, the second term of the GGA potential will require the expensive calculation of the Hessian of the number density ($\nabla^2 n$), so usually a derivative is shifted over to the overlap distribution $\Omega_{\mu\nu}(\boldsymbol{r})$, using integration by parts, giving

$$F^{xc}_{\mu\nu} = \int \left[\frac{\partial\varepsilon_{xc}^{\mathrm{GGA}}}{\partial n}\Omega_{\mu\nu}(\boldsymbol{r}) + 2\left(\frac{\partial\varepsilon_{xc}^{\mathrm{GGA}}}{\partial g}\right)\boldsymbol{\nabla}n\cdot\boldsymbol{\nabla}\Omega_{\mu\nu}(\boldsymbol{r})\right] d^3\boldsymbol{r}. \tag{31}$$

Proceeding as above, the corresponding 2c quantity is found to be

$$\tilde{F}^{2c,xc}_{\mu\nu} = \int \left[\frac{d\varepsilon_{xc}^{\mathrm{GGA}}}{dn}\tilde{\Omega}^{2c}_{\mu\nu}(\boldsymbol{r}) + 2\left(\frac{\partial\varepsilon_{xc}^{\mathrm{GGA}}}{\partial g}\right)\boldsymbol{\nabla}n^{4c}\cdot\boldsymbol{\nabla}\tilde{\Omega}^{2c}_{\mu\nu}(\boldsymbol{r})\right] d^3\boldsymbol{r}. \tag{32}$$

Again using integration by parts, we may recover Eq. (29). These manipulations are thereby seen to commute with the picture-change transformation, albeit only in the exact case. For simplicity we will continue with the form of Eq. (30).

Just as in the case of HF we will argue that, if the 2c calculation is carried out with the correctly transformed overlap distribution $\tilde{\Omega}^{2c}_{\mu\nu}(\boldsymbol{r})$, in addition to the picture-changed one- and two-electron integrals, it will converge to the picture-changed coefficients $\tilde{c}^{2c}$ obtained from the corresponding 4c calculation. However, again the correct decoupling matrix $\boldsymbol{U}$, namely the one associated with the *converged* KS matrix, is not available at the start of calculations and so we will have to seek approximations. One option, pursued by Iakabata and Nakai,[57] is to use the decoupling matrix $\boldsymbol{U}$ associated with the Dirac Hamiltonian instead. The point-wise picture-change transformation of the overlap distribution, even with local approximations, adds significant computational cost, though, and the chosen decoupling matrix $\boldsymbol{U}$ is not optimal. An alternative would be to make picture-change corrections to the number density, starting from

$$\Delta\tilde{n}^{2c}(\boldsymbol{r}) = \tilde{n}^{2c}(\boldsymbol{r}) - n^{2c}(\boldsymbol{r}) = n^{4c}(\boldsymbol{r}) - n^{2c}(\boldsymbol{r}). \tag{33}$$

Due to the local nature of the corrections we would expect these corrections to be separable into atomic contributions, possibly approximated by model densities (see e.g. Refs. 41,42), that is

$$\Delta\tilde{n}^{2c}(\boldsymbol{r}) \simeq \sum_{K=1}^{M} \Delta\tilde{n}^{2c}_{K}(\boldsymbol{r}). \tag{34}$$

Here it is important to stress that the atomic number density n^{2c}_K (without the tilde) is untransformed in the sense that it employs an *untransformed* overlap distribution matrix $\boldsymbol{\Omega}^{2c}_K$, but the *correctly transformed* coefficients $\{\tilde{\boldsymbol{c}}^{2c}_{K,i}\}$ corresponding to the parent 4c atomic calculation. Since we expect $\Delta\tilde{n}^{2c}_K(\boldsymbol{r})$ to be non-zero only in the deep atomic core, one could exploit spherical symmetry by calculating the correction on a *radial* grid. However, we have not pursued this approach, since it still involves point-wise corrections, albeit over a significantly reduced number of integration points.

Instead, we propose the following scheme which integrates nicely with the scheme proposed for HF: for each atomic species K we run a 4c KR fractional occupation KS-calculation which provides the converged atomic KS matrix $\boldsymbol{F}^{4c}_K$. From it we can directly extract the atomic decoupling matrix $\boldsymbol{U}_K$ and the corresponding picture-changed KS-matrix $\tilde{\boldsymbol{F}}^{2c}_K$, notably containing $\tilde{\boldsymbol{F}}^{2c,xc}_K$. We next build the untransformed equivalent

$$F^{2c,xc}_{K;\mu\nu} = \int v^{GGA}_{xc}\left(n^{2c}_K(\boldsymbol{r}), g^{2c}_K(\boldsymbol{r})\right)\Omega^{2c}_{K;\mu\nu}(\boldsymbol{r})\, d^3\boldsymbol{r}, \tag{35}$$

using the correctly picture-changed transformed coefficients $\tilde{\boldsymbol{c}}^{2c}_K$. Our amfX2C picture-change correction to the xc potential is then obtained from atomic quantities as

$$\Delta\tilde{\boldsymbol{F}}^{2c,xc} \simeq \Delta\tilde{\boldsymbol{F}}^{2c,xc}_{\oplus} = \bigoplus_{K=1}^{M} \Delta\tilde{\boldsymbol{F}}^{2c,xc}_K; \qquad \Delta\tilde{\boldsymbol{F}}^{2c,xc}_K = \tilde{\boldsymbol{F}}^{2c,xc}_K - \boldsymbol{F}^{2c,xc}_K. \tag{36}$$

Similarly, the xc energy is corrected by first writing $\tilde{E}^{2c}_{xc} = E^{2c}_{xc} + \Delta\tilde{E}^{2c}_{xc}$, and then seeking an atomic approximation to the correction

$$\Delta\tilde{E}^{2c}_{xc} = \int \varepsilon^{GGA}_{xc}\left(\tilde{n}^{2c}(\boldsymbol{r}), \tilde{g}^{2c}(\boldsymbol{r})\right) d^3\boldsymbol{r} - \int \varepsilon^{GGA}_{xc}\left(n^{2c}(\boldsymbol{r}), g^{2c}(\boldsymbol{r})\right) d^3\boldsymbol{r}. \tag{37}$$

This results in our amfX2C picture-change correction to the xc energy

$$\Delta\tilde{E}^{2c}_{xc} \simeq \Delta\tilde{E}^{2c}_{xc,\oplus} = \sum_{K=1}^{M}\left(\tilde{E}^{2c}_{xc;K} - E^{2c}_{xc;K}\right). \tag{38}$$

At first sight this looks like a rather poor approximation, since, clearly

$$\sum_K \tilde{E}^{2c}_{xc;K} = \sum_K \int \varepsilon^{GGA}_{xc}\left(\tilde{n}^{2c}_K(\boldsymbol{r}), \tilde{g}^{2c}_K(\boldsymbol{r})\right) d^3\boldsymbol{r} \neq \int \varepsilon^{GGA}_{xc}\Big(\sum_K \tilde{n}^{2c}_K(\boldsymbol{r}), \sum_K \tilde{g}^{2c}_K(\boldsymbol{r})\Big) d^3\boldsymbol{r}, \tag{39}$$

due to the general non-linear form of the xc functionals. However, we are calculating picture-change *corrections*, and so one may expect that points for which $\tilde{n}^{2c}_K(\boldsymbol{r}) - n^{2c}_K(\boldsymbol{r})$ deviates significantly from zero for some atomic species K does not overlap with equivalent points for any other species. Under such conditions our approximation becomes perfectly valid due to the local ansatz of the energy density ε_{xc}, cf. Eq. (24).

2. The noncollinear open-shell case

So far, we have discussed the KS amfX2C approach for a closed-shell molecular system which is characterized by a time–reversal symmetric density matrix. Due to the symmetry, the entire dependence of the exchange–correlation energy density reduces for a local-density approximation (LDA) only to the number density (n) [see Eq. (21)], for a generalized-gradient approximation (GGA) also to its gradient, $g_{nn} \equiv (\boldsymbol{\nabla} n)\cdot(\boldsymbol{\nabla} n)$.

The situation is more complex for open-shell systems, where a general Kramers-unrestricted formalism results in a density matrix that has both the time-reversal symmetric (TRS) as well as time-reversal antisymmetric (TRA) component.[6,58] In fact, the latter component gives rise to a non-zero electron spin density, whose z-component (s_z) enters together with its gradient ($\boldsymbol{\nabla} s_z$) into the non-relativistic exchange–correlation energy expression, i.e. $\varepsilon_{xc}^{\mathrm{GGA}} \equiv \varepsilon_{xc}^{\mathrm{GGA}}\big(\{\rho(\boldsymbol{r})\}\big), \rho = n, g_{nn}, s_z, (\boldsymbol{\nabla} s_z\cdot\boldsymbol{\nabla} s_z), (\boldsymbol{\nabla} n\cdot\boldsymbol{\nabla} s_z)$.

However, the presented parametrization of the exchange–correlation energy involving only the z-component of the electron spin density and its gradient is inadequate for theories including the spin–orbit interaction, since the spatial and spin degrees of freedom are no longer independent. Their coupling results in a lack of rotational invariance of the exchange–correlation energy if only z spin-components are involved. This variance can be circumvented by a *noncollinear* parametrization/generalization of the non-relativistic exchange–correlation energy density.

A common noncollinear ansatz follows earlier LDA-based works of Kubler *et al.*,[59] Sandratskii,[60] and van Wuellen[61] where the variable s_z is replaced by its corresponding magnitude $|\boldsymbol{s}|$. Although this extension possesses no numerical problems in the evaluation of exchange–correlation energy, noncollinear potentials and kernels derived from GGA-type functionals are prone to numerical instabilities.[58] A more recent approach, which has been adopted in this work, is based on the noncollinear ansatz proposed by Scalmani and Frisch,[62] where variables depending on the z quantization axis are substituted by more adequate rotationally invariant counterparts:

$$s_z \to s \equiv |\boldsymbol{s}|; \quad (\boldsymbol{\nabla} s_z)\cdot(\boldsymbol{\nabla} s_z) \to g_{ss} \equiv \sum_k (\boldsymbol{\nabla} s_k)\cdot(\boldsymbol{\nabla} s_k); \quad (\boldsymbol{\nabla} n)\cdot(\boldsymbol{\nabla} s_z) \to g_{ns} \equiv f_\nabla g. \tag{40}$$

Here, $k \in x, y, z$; $g \equiv |\boldsymbol{g}|$ with $g_k = (\boldsymbol{\nabla} n)\cdot(\boldsymbol{\nabla} s_k)$, and $f_\nabla = \mathrm{sgn}(\boldsymbol{g}\cdot\boldsymbol{s})$. The noncollinear exchange–correlation energy then reads

$$E_{xc} = \int \varepsilon_{xc}^{\mathrm{GGA}}\big(\{\rho(\boldsymbol{r}\}\big) d^3\boldsymbol{r}, \quad \rho = n, g_{nn}, s, g_{ss}, g_{ns} \tag{41}$$

whereas the noncollinear exchange–correlation potential has the form[58]

$$\begin{aligned} F_{\mu\nu}^{\mathrm{xc}} = \frac{\mathrm{d}E_{xc}}{\mathrm{d}D_{\nu\mu}} = \int \Bigg(& v_{xc}^{n}\,\Omega_{\mu\nu}^{0} + v_{xc}^{s}\sum_k \frac{s_k}{s}\,\Omega_{\mu\nu}^{k} + 2v_{xc}^{g_{nn}}\sum_k (\nabla_k n)\,\nabla_k \Omega_{\mu\nu}^{0} \\ & + 2v_{xc}^{g_{ss}}\sum_{k,l} (\nabla_l s_k)\,\nabla_l \Omega_{\mu\nu}^{k} + v_{xc}^{g_{ns}}\sum_{k,l} f_\nabla \frac{g_k}{g}\left[\,(\nabla_l s_k)\,\nabla_l \Omega_{\mu\nu}^{0} + (\nabla_l n)\,\nabla_l \Omega_{\mu\nu}^{k}\right] \Bigg) d^3\boldsymbol{r}. \end{aligned} \tag{42}$$

Here, $k, l \in x, y, z$ and v_{xc}^{ρ} refer to the partial derivative of $\varepsilon_{xc}^{\mathrm{GGA}}$ with respect to $\rho \in n, g_{nn}, s, g_{ss}, g_{ns}$. $\Omega_{\mu\nu}^{0}$ and $\Omega_{\mu\nu}^{k}$ stand for the overlap and spin distribution functions, respectively, the latter being defined similarly to $\Omega_{\mu\nu}^{0}$ in Eq. (6) as

$$\Omega_{\mu\nu}^{k}(\boldsymbol{r}) \equiv \chi_\mu^\dagger(\boldsymbol{r})\hat{\Sigma}_k\chi_\nu(\boldsymbol{r}) \tag{43}$$

and involves components of the electron spin operator $\hat{\boldsymbol{\Sigma}}$.[58] Note that the evaluation of the exchange–correlation potential in Eq. (42) requires special attention to the limiting cases when the s or g functions approach zero. A detailed description of such a procedure is given in Ref. 58.

C. Extended amfX2C Hamiltonian

Having introduced the amfX2C scheme for both HF and KS mean-field theories, let us conclude this theory section by commenting on some important aspects of the amfX2C scheme, as well as comparing it to existing models for 2ePCE corrections. Ultimately, the discussion leads to the introduction of an extended amfX2C model, dubbed eamfX2C, which has the potential to outperform the amfX2C model, for instance, in properly treating long-range Coulomb interactions in solids.

Algorithm 1 Pseudo-code highlighting the essential steps for the amfX2C approach.

1: /* Initialize the molecular two-electron (2e) Fock matrices and XC energy */
2: $\boldsymbol{F}^{4c,2e}_{\oplus} = \boldsymbol{0}$; $\Delta\tilde{\boldsymbol{F}}^{2c,2e}_{\oplus} = \boldsymbol{0}$; $\Delta\tilde{E}^{2c}_{xc,\oplus} = 0$
3: **for all** `unique atom types` $K \in$ `molecule` **do**
4: Let $\{\mu,\nu\} \in$ atomic basis K
5: /* Solve the 4c SCF equation */
6: $\boldsymbol{F}^{4c}_K \boldsymbol{c}^{4c}_K = \boldsymbol{c}^{4c}_K \epsilon^{4c}_K$ with $F^{4c}_{K,\mu\nu} = \begin{cases} F^{4c,HF}_{K,\mu\nu}[\boldsymbol{D}^{4c}_K] = h^{4c}_{K,\mu\nu} + \sum_{\gamma,\delta\in K} G^{4c}_{\mu\nu,\gamma\delta} D^{4c}_{K,\delta\gamma} \\ F^{4c,KS}_{K,\mu\nu}[\boldsymbol{D}^{4c}_K] = h^{4c}_{K,\mu\nu} + \sum_{\gamma,\delta\in K} G^{\omega,4c}_{\mu\nu,\gamma\delta} D^{4c}_{K,\delta\gamma} + F^{4c,xc}_{K,\mu\nu}[\boldsymbol{D}^{4c}_K] \end{cases}$
7: /* Add K-th atomic 2e Fock contrib. $\boldsymbol{F}^{4c,2e}_K$ to the corresponding molecular block */
8: $\boldsymbol{F}^{4c,2e}_{\oplus} \leftarrow \boldsymbol{F}^{4c,2e}_K$ with $F^{4c,2e}_{K,\mu\nu} = \begin{cases} F^{4c,HF}_{K,\mu\nu}[\boldsymbol{D}^{4c_K}] - h^{4c}_{K,\mu\nu} \\ F^{4c,KS}_{K,\mu\nu}[\boldsymbol{D}^{4c}_K] - h^{4c}_{K,\mu\nu} \end{cases}$
9: /* Evaluate the atomic X2C decoupling matrix $\boldsymbol{U}_K$ from $\boldsymbol{F}^{4c}_K$ and calculate */
10: $\tilde{\boldsymbol{D}}^{2c}_K = \left[\boldsymbol{U}^\dagger_K \boldsymbol{D}^{4c}_K \boldsymbol{U}_K\right]^{LL}$; $\Delta\tilde{\boldsymbol{F}}^{2c,2e}_K = \left[\boldsymbol{U}^\dagger_K \boldsymbol{F}^{4c,2e}_K \boldsymbol{U}_K\right]^{LL} - \boldsymbol{F}^{2c,2e}_K$
11: /* where the latter term facilitates untransformed quantities G^{2c}, $G^{\omega,2c}$, and $F^{2c,xc}_K$ */
12: $F^{2c,2e}_{K,\mu\nu} = \begin{cases} F^{2c,2e,HF}_{K,\mu\nu}[\tilde{\boldsymbol{D}}^{2c}_K] = \sum_{\gamma,\delta\in K} G^{2c}_{\mu\nu,\gamma\delta} \tilde{D}^{2c}_{K,\delta\gamma} \\ F^{2c,2e,KS}_{K,\mu\nu}[\tilde{\boldsymbol{D}}^{2c}_K] = \sum_{\gamma,\delta\in K} G^{\omega,2c}_{\mu\nu,\gamma\delta} \tilde{D}^{2c}_{K,\delta\gamma} + F^{2c,xc}_{K,\mu\nu}[\tilde{\boldsymbol{D}}^{2c}_K] \end{cases}$
13: /* Add K-th atomic block of the picture-change error correction to the corresponding molecular block. In case of DFT, add also the atomic XC energy correction: */
14: $\Delta\tilde{\boldsymbol{F}}^{2c,2e}_{\oplus} \leftarrow \Delta\tilde{\boldsymbol{F}}^{2c,2e}_K$; $\Delta\tilde{E}^{2c}_{xc,\oplus} \leftarrow \left(E^{4c}_{xc,K}[\boldsymbol{D}^{4c}_K] - E^{2c}_{xc,K}[\tilde{\boldsymbol{D}}^{2c}_K]\right)$
15: **end for**
16: Let $\{\mu,\nu\} \in$ full molecular basis
17: /* Evaluate the molecular X2C decoupling matrix $\boldsymbol{U}$ from */
18: $\tilde{\boldsymbol{h}}^{4c} = \boldsymbol{h}^{4c} + \boldsymbol{F}^{4c,2e}_{\oplus}$
19: /* Solve the 2c SCF equation with the amfX2C Fock matrix operator */
20: $\boldsymbol{F}^{2c}\boldsymbol{c}^{2c} = \boldsymbol{c}^{2c}\epsilon^{2c}$ with $F^{2c}_{\mu\nu} \equiv F^{amfX2C}_{\mu\nu} = \underbrace{\left[\boldsymbol{U}^\dagger \boldsymbol{h}^{4c} \boldsymbol{U}\right]^{LL}_{\mu\nu} + \Delta\tilde{F}^{2c,2e}_{\oplus,\mu\nu}}_{\text{static terms}} + \underbrace{F^{2c,2e}_{\mu\nu}[\boldsymbol{D}^{2c}]}_{\text{dynamic term}}$

We start by noting that: (i) in contrast to Liu and Cheng[34] our amfX2C scheme allows to take into account PCE corrections for both *spin-independent* and *spin-dependent* parts of the two-electron interaction; (ii) the proposed amfX2C approach has the additional appealing feature that it allows its straightforward extension to a KS-DFT framework as discussed in Section II B; (iii) the algebraic nature of amfX2C also allows an easy extraction of 2ePCE corrections not only from the common 2e Coulomb interaction term but also from more elaborate Gaunt and Breit 2e-interaction terms; (iv) the 2ePCE corrections are only introduced in the atomic diagonal blocks. This further implies:

- The 2ePCE corrections will not contribute to the molecular gradient.
- The direct 2e Coulomb contribution will not cancel exactly the electron-nucleus interaction at long distance from atomic centers that potentially prevents a direct application of amfX2C in solid-state calculations. This issue was discussed for instance by van Wüllen and Michauk, and solved by building the former contributions using a superposition of atomic model densities[41], although such a scheme does not accommodate HF exchange contributions.

In order to overcome the latter, particular shortcoming of the amfX2C model, we additionally propose a modified amfX2C model which exploits a superposition of atomic density matrices (expressed in AO-basis). The resulting *extended* amfX2C model (eamfX2C) is summarized in Alg. 2. Most importantly, in contrast to the amfX2C model, where we assemble a molecular 4c Fock matrix $\boldsymbol{F}^{4c}_{\oplus}$ from atomic building blocks (see line 8 in Alg. 1), this task is replaced in the eamfX2C algorithm by the buildup of a molecular *density* matrix $\boldsymbol{D}^{4c}_{\oplus}$ from atomic density matrices as indicated in line 10 of Alg. 2. The latter construction therefore entails the evaluation of a two-electron (KS-)Fock matrix contribution in the *full* molecular basis within a 4c framework (c.f. line 14 of Alg .2) which is absent in the molecular computational panel (lower part of Alg. 1) of the simpler amfX2C model. Although introducing such a

requirement seems odd at a first glance, in particular, with regard to the computational scaling, let us recall that an efficient density-based screening in the two-electron (KS-)Fock matrix construction will enable a calculation of the term $F_{\mu\nu}^{4c,2e}[\boldsymbol{D}_{\oplus}^{4c}]$ at a fractional cost of a regular two-electron (KS-)Fock matrix evaluation because of the sparsity associated with the molecular density matrix $\boldsymbol{D}_{\oplus}^{4c}$. In this regard, one can recognize a similarity between the eamfX2C scheme and the atomic initial guess proposed by van Lenthe and co-workers[63] where the initial Fock matrix is formed from a superposition of atomic density matrices. Moreover, in the KS-DFT framework, one can also easily obtain the xc energy picture-change correction (Alg. 2, line 23) from contributions evaluated in the full *molecular* basis,

$$\Delta\tilde{E}_{xc}^{2c} \simeq \tilde{E}_{xc,\oplus}^{2c} = E_{xc}^{4c}[\boldsymbol{D}_{\oplus}^{4c}] - E_{xc}^{2c}[\tilde{\boldsymbol{D}}_{\oplus}^{2c}] \;, \tag{44}$$

in contrast to the correction term $\Delta\tilde{E}_{xc}^{2c}$ of the amfX2C model (Alg. 1, line 14) which consists of a sum of K contributions each calculated in the K-th *atomic* basis.

D. A remark on notations

Since the combination of a several 2ePCE correction models with a multiple defining Hamiltonians for obtaining the unitary decoupling matrix $\boldsymbol{U}$ may easily lead to confusion, we have decided to introduce a notation for X2C Hamiltonians where the 2ePCE correction model is given as a prefix a while the defining Hamiltonian matrix $\boldsymbol{h}_{\mathrm{def}}^{4c}$ is given as subscript b, that is: aX2C$_{\mathrm{b}}$.

In particular we have

$$\mathrm{a} = \begin{cases} \text{1e} & \textbf{if} \text{ no 2ePCE corrections added: } \Delta\tilde{\boldsymbol{F}}^{2c,2e} = \boldsymbol{0} \\ \text{amf} & \textbf{if} \text{ atomic–mean field 2ePCE corrections added: } \Delta\tilde{\boldsymbol{F}}^{2c,2e} \simeq \Delta\tilde{\boldsymbol{F}}_{\oplus}^{2c,2e} \text{ (see line 14 in Alg. 1)} \\ \text{eamf} & \textbf{if} \text{ extended atomic–mean field 2ePCE corrections added: } \Delta\tilde{\boldsymbol{F}}^{2c,2e} \simeq \Delta\tilde{\boldsymbol{F}}_{\oplus}^{2c,2e} \text{ (see line 19 in Alg. 2)} \\ \text{AMFI} & \textbf{if} \text{ atomic–mean field first–order (DKH1) spin–orbit 2ePCE corrections added: see Refs. 37 and 38} \\ \text{mmf} & \textbf{if} \text{ post-SCF molecular–mean field 2ePCE corrections added: see Ref. 32} \end{cases}$$

and

$$\mathrm{b} = \begin{cases} \text{D} & \textbf{if } \boldsymbol{U} \text{ is evaluated from } \boldsymbol{h}_{\mathrm{def}}^{4c} \equiv \boldsymbol{h}^{4c} \text{ where } \boldsymbol{h}^{4c} \text{ is the one-electron Dirac Hamiltonian} \\ \text{DC} & \textbf{if } \boldsymbol{U} \text{ is evaluated from } \boldsymbol{h}_{\mathrm{def}}^{4c} \equiv \boldsymbol{h}^{4c} + \boldsymbol{F}_{\oplus}^{4c,2e} \text{ with Coulomb integrals contributing to } \boldsymbol{F}_{\oplus}^{4c,2e} \\ \text{DCG} & \textbf{if } \boldsymbol{U} \text{ is evaluated from } \boldsymbol{h}_{\mathrm{def}}^{4c} \equiv \boldsymbol{h}^{4c} + \boldsymbol{F}_{\oplus}^{4c,2e} \text{ with Coulomb–Gaunt integrals contributing to } \boldsymbol{F}_{\oplus}^{4c,2e} \\ \text{DCB} & \textbf{if } \boldsymbol{U} \text{ is evaluated from } \boldsymbol{h}_{\mathrm{def}}^{4c} \equiv \boldsymbol{h}^{4c} + \boldsymbol{F}_{\oplus}^{4c,2e} \text{ with Coulomb–Breit integrals contributing to } \boldsymbol{F}_{\oplus}^{4c,2e}. \end{cases}$$

III. COMPUTATIONAL DETAILS

If not stated otherwise, all calculations reported in this work have been carried out by both DIRAC[5] and RESPECT[6] programs, making use of a common computational setup: (i) a finite value for the speed of light $c = 137.03599907400\ a_0E_h/\hbar$,[64] (ii) a point nucleus model for all atomic nuclei to ease comparison between data obtained by the programs, (iii) an explicit inclusion of $(SS|SS)$-type electron repulsion AO-integrals, (iv) atom-centered uncontracted Gaussian-type basis sets of double-ζ quality (dyall.v2z, dubbed `v2z`) for each unique atom type,[65–72] (v) DIRAC's default numerical integration grids consisting of the basis-set adaptive radial quadrature by Lindh *et al.*,[73] and the angular quadrature by Lebedev[74–76] (to achieve consistent exchange–correlation PCE corrections by both programs, it turned out be crucial to use integration grids of identical composition and quality) and (vi) a threshold for SCF convergence of 10^{-7} in the DIIS[77] error vector. All atomic and molecular calculations with DIRAC were performed within a Kramers-restricted (KR) formalism, employing for open-shell systems either an average-of-configuration (AOC) approach[53] (HF) or a fractional occupation (FO) approach (KS-DFT). In the case of group-16 diatomics (chalcogenide series), AOC HF calculations take into account all possible configurations of six electrons in 8 Kramers-paired spinors (i.e., representing the π, π^* valence shells). In RESPECT, molecular open-shell calculations were performed within a Kramers-unrestricted (KU) formalism,[6] whereas atomic results were obtained with the KR FO approach, both for HF and KS-DFT calculations. All KS-DFT calculations were carried out with either a PBE or PBE0 exchange–correlation functional.[78–80]

Algorithm 2 Pseudo-code highlighting the essential steps for the eamfX2C approach.

/* Initialize the molecular effective density matrices */

$\boldsymbol{D}^{4c}_{\oplus} = \boldsymbol{0}$; $\tilde{\boldsymbol{D}}^{2c}_{\oplus} = \boldsymbol{0}$

for all `unique atom types` $K \in$ `molecule` **do**

  Let $\{\mu, \nu\} \in$ atomic basis K

  /* Solve the 4c SCF equation */

  $\boldsymbol{F}^{4c}_K \boldsymbol{c}^{4c}_K = \boldsymbol{c}^{4c}_K \epsilon^{4c}_K$ with $F^{4c}_{K,\mu\nu} = \begin{cases} F^{4c,HF}_{K,\mu\nu}[\boldsymbol{D}^{4c}_K] = h^{4c}_{K,\mu\nu} + \sum\limits_{\gamma,\delta\in K} G^{4c}_{\mu\nu,\gamma\delta} D^{4c}_{K,\delta\gamma} \\ F^{4c,KS}_{K,\mu\nu}[\boldsymbol{D}^{4c}_K] = h^{4c}_{K,\mu\nu} + \sum\limits_{\gamma,\delta\in K} G^{\omega,4c}_{\mu\nu,\gamma\delta} D^{4c}_{K,\delta\gamma} + F^{4c,xc}_{K,\mu\nu}[\boldsymbol{D}^{4c}_K] \end{cases}$

  /* Evaluate the atomic X2C decoupling matrix $\boldsymbol{U}_K$ from $\boldsymbol{F}^{4c}_K$ and calculate */

  $\tilde{\boldsymbol{D}}^{2c}_K = \left[\boldsymbol{U}^\dagger_K \boldsymbol{D}^{4c}_K \boldsymbol{U}_K\right]^{LL}$

  /* Add K-th atomic effective density matrices $\boldsymbol{D}^{4c}_K$ and $\tilde{\boldsymbol{D}}^{2c}_K$ to the molecular block */

  $\boldsymbol{D}^{4c}_{\oplus} \leftarrow \boldsymbol{D}^{4c}_K$; $\tilde{\boldsymbol{D}}^{2c}_{\oplus} \leftarrow \tilde{\boldsymbol{D}}^{2c}_K$

end for

Let $\{\mu, \nu\} \in$ full molecular basis

/* Evaluate the molecular 4c 2e Fock matrix $\boldsymbol{F}^{4c,2e}_{\oplus}$ with elements */

$F^{4c,2e}_{\oplus,\mu\nu} = \begin{cases} F^{4c,2e,HF}_{\oplus,\mu\nu}[\boldsymbol{D}^{4c}_{\oplus}] = \sum\limits_{\gamma,\delta} G^{4c}_{\mu\nu,\gamma\delta} D^{4c}_{\oplus,\delta\gamma} \\ F^{4c,2e,KS}_{\oplus,\mu\nu}[\boldsymbol{D}^{4c}_{\oplus}] = \sum\limits_{\gamma,\delta} G^{\omega,4c}_{\mu\nu,\gamma\delta} D^{4c}_{\oplus,\delta\gamma} + F^{4c,xc}_{\mu\nu}[\boldsymbol{D}^{4c}_{\oplus}] \end{cases}$

/* If DFT, evaluate also the molecular xc energy $E^{4c}_{xc}[\boldsymbol{D}^{4c}_{\oplus}]$ */

/* Evaluate the molecular X2C decoupling matrix $\boldsymbol{U}$ from */

$\tilde{\boldsymbol{h}}^{4c} = \boldsymbol{h}^{4c} + \boldsymbol{F}^{4c,2e}_{\oplus}$

/* Determine the molecular 2e picture-change transformation correction as */

$\Delta\tilde{\boldsymbol{F}}^{2c,2e}_{\oplus} = \left[\boldsymbol{U}^\dagger \boldsymbol{F}^{4c,2e}_{\oplus} \boldsymbol{U}\right]^{LL} - \boldsymbol{F}^{2c,2e}$

where

$F^{2c,2e}_{\mu\nu} = \begin{cases} F^{2c,2e,HF}_{\mu\nu}[\tilde{\boldsymbol{D}}^{2c}_{\oplus}] = \sum\limits_{\gamma,\delta} G^{2c}_{\mu\nu,\gamma\delta} \tilde{D}^{2c}_{\oplus,\delta\gamma} \\ F^{2c,2e,KS}_{\mu\nu}[\tilde{\boldsymbol{D}}^{2c}_{\oplus}] = \sum\limits_{\gamma,\delta} G^{\omega,2c}_{\mu\nu,\gamma\delta} \tilde{D}^{2c}_{\oplus,\delta\gamma} + F^{2c,xc}_{\mu\nu}[\tilde{\boldsymbol{D}}^{2c}_{\oplus}] \end{cases}$

/* If DFT, determine also the molecular PCE correction to the xc energy as */

$\Delta\tilde{E}^{2c}_{xc,\oplus} = E^{4c}_{xc}[\boldsymbol{D}^{4c}_{\oplus}] - E^{2c}_{xc}[\tilde{\boldsymbol{D}}^{2c}_{\oplus}]$

/* Solve the 2c SCF equation with the eamfX2C Fock matrix operator */

$\boldsymbol{F}^{2c}\boldsymbol{c}^{2c} = \boldsymbol{c}^{2c}\epsilon^{2c}$ with $F^{2c}_{\mu\nu} \equiv F^{eamfX2C}_{\mu\nu} = \underbrace{\left[\boldsymbol{U}^\dagger \boldsymbol{h}^{4c} \boldsymbol{U}\right]^{LL}_{\mu\nu} + \Delta\tilde{F}^{2c,2e}_{\oplus,\mu\nu}}_{\text{static terms}} + \underbrace{F^{2c,2e}_{\mu\nu}[\boldsymbol{D}^{2c}]}_{\text{dynamic term}}$

Table I: Structural parameters of the group 16 (left-hand side) and group 18 diatomics (right-hand side) considered in this work. All internuclear distances are given in Å.

molecule	r_{X-X}	Reference	molecule	r_{X-X}	Reference
			He_2	2.970	81
O_2	1.20752	83	Ne_2	3.091	81
S_2	1.889	83	Ar_2	3.756	81
Se_2	2.166	83	Kr_2	4.008	81
Te_2	2.557	83	Xe_2	4.363	81
Po_2	2.795	83	Rn_2	4.427	82
Lv_2	3.230	84	Og_2	4.329	82

For the lighter noble gas dimers, internuclear distances were taken from experimentally available data[81] whereas for the heavier homologues Rn_2 and Og_2, respectively, computationally optimized structures were taken from Ref. 82. Similarly, in the case of the chalcogene series, all geometries were taken from Ref. 83, except for the heaviest diatomic system Lv_2 for which the internuclear distance of $R_e = 3.230$ Å was extracted by visual inspection from Figure 1 of Ref. 84. Table I summarizes the structural parameters for all group 16 and group 18 diatomics employed in this work.

In the case of the methane molecule CH_4 discussed in Section IV A 3, we assumed a T_d-symmetrical molecular

framework with a C-H internuclear distance of 1.091 Å and a <H-C-H bond angle of 109.471 degrees. In order to enhance relativistic effects, we scaled down the speed of light c by a factor of 10, corresponding to an actual value of $c_{\text{scaled}} = 13.703599907400\ a_0 E_h/\hbar$, for both the atomic as well as the molecular calculations.

The absolute contact densities and contact density shifts for selected (closed-shell) copernicium fluorides (CnF_n, $n = 0, 2, 4, 6$), discussed in Section IV B, were calculated from mean-field HF wave functions employing a 4c Dirac-Coulomb as well as the X2C Hamiltonian supplemented with various 2ePCE corrections. The structures for each of the copernicium fluorides were optimized within a 4c Dirac-Coulomb framework by means of KS-DFT calculations employing the PBE0 exchange-correlation functional. Following the very recent work of Hu and Zou,[85] we assumed for the structure optimization a linear ($n = 2$), square-planar ($n = 4$) and octahedral ($n = 6$) geometry for the respective copernicium fluorides CnF_n. The resulting equilibrium Cn-F internuclear distances are compiled in Table X along with the corresponding double-group symmetry. It is worthwhile to note that, given that the primary concern of our the present study is not to provide an accurate computation of the contact density with respect to a converged basis set saturation at the heavy nuclei Cn, we did not further pursue any further augmentation of the set of primitives in the basis set as, for example, done in our earlier works in Refs. 86 and 87. Moreover, as we aim within the e(amf)X2C models to reproduce as accurate as possible the parent four-component results, computational details for the the two-component calculations have to match the corresponding ones for four-component reference calculations. Hence, any considerations for convergence in the basis set, crucial to obtain quantitatively converged contact densities, hold simultaneously in both cases, that is, in a four-component and a two-component framework.

Finally, Section IV C comprises an assessment of the accuracy and suitability of various 2c approaches to adequately describe (absolute) K- and L-edge core-ionization energies as well as L_3-L_2 edge spin-orbit splittings, denoted as Δ_L^{SO}, for heavy d- and p-block compounds. To this end, we considered one atomic anion (At^-) and two anionic and neutral molecular cases, respectively. In the former case we employed the same computational setup for the SCF and EOM-CCSD[88] calculations as described in full detail in Ref. 89 which provides high-quality computational reference data. In the remaining molecular examples, we employed for CnF_6 the optimized molecular structure listed in Table X, while for $[Au(Cl)_4]^-$ the optimized molecular structure has been taken from Table 1 (column MP2/aug-cc-pVTZ) in Ref. 90. In either molecular cases, we correlated for the EOM-CCSD step all electrons and introduced an energy-based cutoff in the virtual spinor space at 3 Hartree making use of the dyall.v2z basis sets for all atom types. Since we are solely interested in a genuine comparison of different two-component Hamiltonian models rather than achieving *quantitatively converged* results for the K-, L-edge and M-edge (the latter only for the [Au]-complex) ionisation potentials which would call for, for example, to make use of tailored basis sets[91], the latter motivates for the present work our choice to merely aim at a *qualitative* electron correlation treatment.

IV. RESULTS AND DISCUSSION

In this section we will critically assess the accuracy of our newly developed 2ePCE correction approaches for all-electron X2C HF and DFT calculations in the two major, common use cases, that is (i) with a variational account of SO interaction as well as (ii) in a genuine spin-free SC framework. A detailed summary of the notation of the 2ePCE correction applied to the X2C Hamiltonian can be found in Section II D.

In Section IV A, we commence with a discussion of the spinor energies of Og_2, a prototypical, closed-shell superheavy diatomic molecule, optimized both within a mean-field HF and a KS-DFT computational model (Section IV A 1). Results for the lighter homologues of the corresponding group 18 diatomics can be found in the public research repository ZENODO (see Section V for more details). Along the same lines and as an example of an open-shell diatomic molecule, we consider in Section IV A 2 the case of Te_2 as a representative of the group-16 diatomics. Results for the remaining group-16 diatomics listed in Table I can also be found in the ZENODO repository (see Section V for more details). To conclude the discussion on total as well as spinor energies, we assess in Section IV A 3 the numerical performance of our selection of PCE-corrected X2C models for the case of an "ultrarelativistic" methane molecule employing a ten-fold reduced speed of light c, that is $c/10$.

Next, in Section IV B we evaluate the suitability of our (e)amf-X2C models for the calculation of absolute contact densities at a heavy nuclear center and, equally important, for contact density *shifts*. The latter play, for example, an important role in computational models for the determination of isomer shifts that are accessible in experimental Mössbauer spectroscopy. To this end, we perform contact density calculations for a series n (with $n = 0, 2, 4, 6$) of fluoride compounds of the heaviest group 12 member Cn, ranging from the bare Cn atom to the hexafluoride CnF_6.

In Section IV C we conclude our assessment by focusing on the calculation of correlated X-ray core ionization energies. Besides the At^- mono-anion for which benchmark data is available in the literature,[89] we consider two molecular applications of $5d$ and $6d$-containing molecules by taking advantage of the recently developed EOM-CCSD approach for core spectroscopy.[89]

Table II: SCF total energy (E) and spinor energies of selected doubly-degenerate occupied spinors (ϵ) for Og_2 as obtained from HF/v2z calculations within a four-component Dirac-Coulomb (^{4}DC) as well as a two-component Hamiltonian framework, including the new (e)amfX2C$_{DC}$ models. All energies are given in Hartree.

	1eX2C$_D$	AMFIX2C$_D$	amfX2C$_{DC}$	eamfX2C$_{DC}$	^{4}DC
E	-110045.25693	-110015.96688	-110116.09102	-110116.09102	-110116.09101
ϵ_{1-2}	-8248.36274	-8248.69505	-8272.12530	-8272.12529	-8272.12529
ϵ_{3-4}	-1733.89154	-1734.00101	-1738.99764	-1738.99763	-1738.99763
ϵ_{5-6}	-1693.29607	-1683.36133	-1686.06374	-1686.06374	-1686.06374
ϵ_{7-10}	-1133.93651	-1136.41886	-1137.97905	-1137.97904	-1137.97904
ϵ_{11-12}	-474.97349	-475.01315	-476.18010	-476.18010	-476.18010
ϵ_{13-14}	-454.67004	-452.30145	-452.93331	-452.93331	-452.93331
ϵ_{15-18}	-317.10573	-317.76956	-318.14142	-318.14142	-318.14142
ϵ_{19-22}	-287.84702	-286.46016	-286.46862	-286.46861	-286.46861
ϵ_{23-28}	-264.51100	-265.35539	-265.51476	-265.51476	-265.51476
ϵ_{29-30}	-142.09699	-142.11136	-142.43246	-142.43246	-142.43246
ϵ_{31-32}	-131.90002	-131.20172	-131.36462	-131.36462	-131.36462
ϵ_{33-36}	-91.64727	-91.85115	-91.94818	-91.94818	-91.94818
ϵ_{37-40}	-76.61348	-76.20853	-76.19682	-76.19682	-76.19682
ϵ_{41-46}	-70.00892	-70.25753	-70.28799	-70.28799	-70.28799
ϵ_{47-52}	-50.08877	-49.76060	-49.73704	-49.73703	-49.73703
ϵ_{53-60}	-47.74819	-47.99085	-47.99004	-47.99004	-47.99004
...	...	...	...	...	...
ϵ_{110}	-1.47090	-1.48271	-1.48161	-1.48162	-1.48162
ϵ_{111}	-1.31383	-1.31314	-1.31699	-1.31698	-1.31698
ϵ_{112}	-1.31254	-1.31185	-1.31572	-1.31571	-1.31571
ϵ_{113}	-0.74647	-0.73730	-0.73819	-0.73819	-0.73819
ϵ_{114}	-0.74381	-0.73455	-0.73545	-0.73545	-0.73545
ϵ_{115}	-0.31691	-0.31826	-0.31821	-0.31822	-0.31822
ϵ_{116}	-0.30372	-0.30516	-0.30512	-0.30512	-0.30512
ϵ_{117}	-0.29260	-0.29413	-0.29411	-0.29411	-0.29411
ϵ_{118}	-0.28036	-0.28196	-0.28194	-0.28193	-0.28193

A. Spinor energies of (super)heavy diatomic molecules

1. Closed-shell Og_2

In the following, we will assess the numerical performance of our atomic mean-field PCE correction model and its extended version within the context of an exact two-component decoupling approach by considering as prime example the heaviest group-18 dimer, namely Og_2. Since the molecule is closed-shell in its electronic ground state, both the Kramers-restricted and the Kramers-unrestricted SCF formalism implemented in DIRAC and ReSpect, respectively, converge to the same solution. In order to underline the importance of a simultaneous treatment of 2eSC and 2eSO PCE corrections within the X2C Hamiltonian framework, we compile in Table II a selected set of HF spinor energies for Og_2, ranging from the inner- to outer-core as well as to the valence region, and compare the various X2C-based spinor energies with the 4c Dirac-Coulomb reference data (^{4}DC; sixth column in Table II). In addition, the left panel of Figure 1 comprises the HF-based deviations for SO splittings of the inner-core and outer-core shells of Og_2 with predominant atomic-like character illustrated for results obtained with the various two-component Hamiltonian schemes listed in Table II by comparison to the ^{4}DC reference. Finally, the right panel of Figure 1 provides a similar comparison for a correlated KS-DFT-based approach employing the PBE functional where the underlying absolute energies are summarized in Table III.

a. HF In line with previous works,[31,41] we find the largest deviations within an X2C framework from the reference 4c spinor energies in an HF approach for the innermost s and p shells where 2eSO (p shells) and 2eSC PCE corrections (s and p shells) are expected to be of utmost importance (see also the discussion of core-ionization energies in Section IV C). Hence, considering first the bare one-electron X2C (second column, 1eX2C$_D$ in Table II), which ignores 2e picture changes altogether, we encounter deviations up to +23.8 Hartree with respect to the four-component reference data for the innermost s shells and up to -7.2 Hartree for the lowest-lying p shells. Next, by taking into account atomic SO mean-field PCE corrections within the AMFI model (third column, AMFIX2C$_D$) results in a minor improvement of about -0.4 Hartree for the inner s shells while the lowest-lying p shells become destabilized through the PCE corrections by about +10 Hartree leading to a deviation of $\approx$ +2.7 Hartree wrt the corresponding 4c reference values.

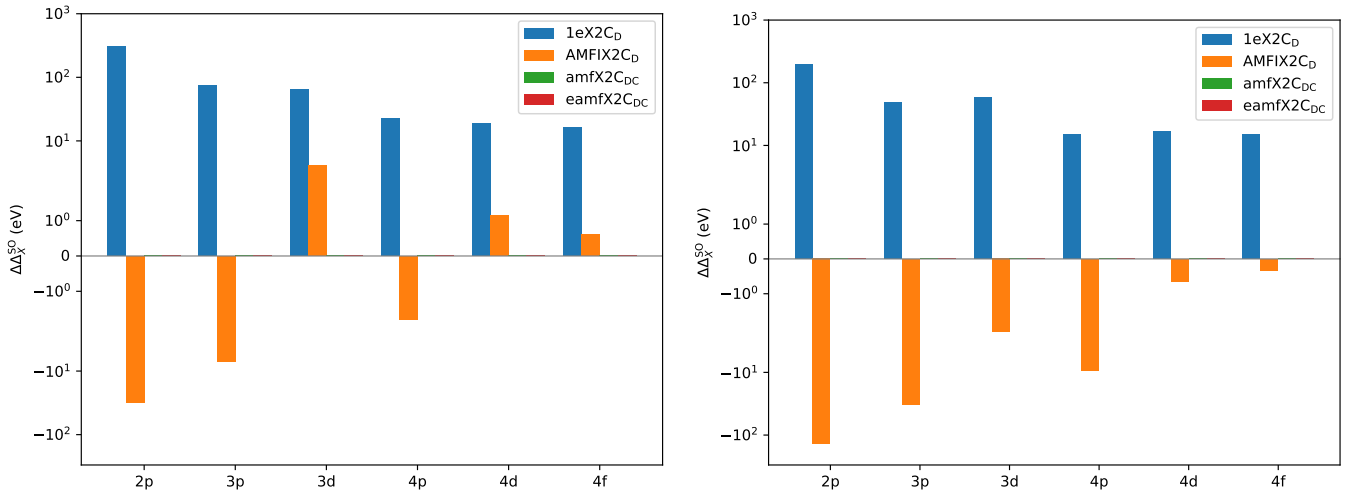

(a) HF (b) DFT/PBE

Figure 1: Differences of spin-orbit splittings (Δ_X^{SO}) of the inner-core to outer-core Og-atomic-like shells in Og_2 with respect to the ^{4}DC reference values either within a HF approach (panel (a)) or a DFT/PBE approach (panel (b)). All data is compiled from the SCF spinor energies listed in Tables II and III, respectively. Energy differences are given in eV. Note that errors associated with the (e)amfX2C models are not visible in the figures.

By contrast, both our amfX2C$_{DC}$ and eamfX2C$_{DC}$ PCE correction schemes for the X2C Hamiltonian yield spinor energies which merely differ by 10 μHartree or less for the innermost s shells – and likewise for the p shells – of Og_2 from the 4c reference data. These findings strikingly illustrate the excellent numerical performance of our newly proposed amf-based 2eSC- and 2eSO-PCE corrections applied in a molecular framework. Moreover, in particular in the core region close to a (heavy) nucleus, SO splittings are a crucial measure since they probe the ability of PCE-corrected 2c schemes to provide *quantitative relative* energies. Here, calculations employing the 1eX2C$_{rmD}$ as well as the AMFIX2C$_D$ Hamiltonian yield SO-splittings for the atomic-like shells ($\Delta_X^{SO}, X = p, d, f$ obtained as energy difference $\epsilon_{X_{(2l+1)/2}} - \epsilon_{X_{(2l-1)/2}}$) in Og_2 which deviate significantly from the ^{4}DC reference data as illustrated in Figure 1a with data obtained from Table II. For example, for the bare 1eX2C$_D$ approach we find deviations in Δ_X^{SO} of up to $\approx +11.3$ Hartree for the $2p$ shell which corresponds to an overestimation of the splitting by $\approx 2\%$. Moving to outer-core shells, the overestimation of the SO splitting Δ^{SO} becomes even worse with deviations as large as $\approx +25\%$ for Δ_{4f}^{SO}. As can be seen from Figure 1a, the latter deviations can be reduced significantly for all inner- and outer-core spin-orbit-split shells through the introduction of AMFI-based SO mean-field PCE corrections within AMFIX2C$_D$. Finally, as it is evident from the matching *absoulute* spinor energies discussed above, all SO splittings considered in Figure 1a obtained within our (e)amfX2C$_{DC}$ Hamiltonian frameworks match (within significant digits) their 4c reference data (errors are therefore not visible in the Figure), underlining once more the importance of taking into account both 2eSC- and 2eSO-PCE corrections in an X2C many-electron Hamiltonian framework.

In passing we note that the numerical performance of our (e)amfX2C models not only holds for the inner- and outer-core but also for the correspondings valence shells ($\epsilon_{110-118}$ in Table II) of the diatomic Og_2 where the ^{4}DC and (e)amfX2C$_{DC}$ data essentially remains indistinguishable within significant digits. Noteworthy, in the (outer-)valence region, the AMFIX2C$_D$ approach leads to absolute spinor energies which differ by less than 10^{-3} Hartree from their reference values. Hence, the latter may explain why this PCE correction scheme has successfully been applied in the past in numerous numerical applications that particularly probed valence-dominated properties. Finally, our data in Table II further shows that neglecting PCE corrections at all results even for valence spinors in absolute errors for the spinor energies on the order of 10^{-2} Hartree.

b. DFT/PBE What about the numerical performance of our (e)amf PCE correction models in a correlated framework? To this end, we consider in the following the same prime superheavy diatomic molecular system Og_2 (*vide supra*) within a DFT/PBE-based SCF approach. A particularity of our (e)amf PCE correction models is rooted in the fact that, as illustrated in Algorithms 1 and 2, respectively, both models enable not only a basis-set dependent but also a *self-consistent-field model dependent* PCE correction which originate from the specific contributions that enter the corresponding 2e Fock matrices. The latter implies that our (e)amf PCE correction models provide tailor-made PCE corrections which explicitly account for the subtleties that arise from the employed exchange-correlation

Table III: SCF total energy (E) and spinor energies (ϵ) of the doubly-degenerate occupied spinors for Og_2 as obtained from DFT/PBE/v2z calculations within a four-component Dirac-Coulomb (^{4}DC) as well as a two-component Hamiltonian framework, including the new (e)amfX2C$_{DC}$ models. All energies are given in Hartree.

	1eX2C$_D$	AMFIX2C$_D$	amfX2C$_{DC}$	eamfX2C$_{DC}$	^{4}DC
E	-110101.19289	-110071.81703	-110191.68717	-110191.68717	-110191.68716
ϵ_{1-2}	-8194.40021	-8194.74358	-8228.57826	-8228.57826	-8228.57826
ϵ_{3-4}	-1714.66379	-1714.76764	-1720.61964	-1720.61964	-1720.61964
ϵ_{5-6}	-1675.00848	-1665.13958	-1672.43570	-1672.43570	-1672.43570
ϵ_{7-10}	-1119.86023	-1122.32402	-1124.50368	-1124.50367	-1124.50367
ϵ_{11-12}	-465.42115	-465.45560	-466.74289	-466.74289	-466.74289
ϵ_{13-14}	-445.52684	-443.18339	-444.87850	-444.87850	-444.87849
ϵ_{15-18}	-309.80499	-310.45933	-310.94433	-310.94433	-310.94433
ϵ_{19-22}	-281.43839	-280.06878	-280.35730	-280.35730	-280.35730
ϵ_{23-28}	-258.40460	-259.23760	-259.44279	-259.44279	-259.44279
ϵ_{29-30}	-137.01495	-137.02661	-137.36644	-137.36644	-137.36644
ϵ_{31-21}	-127.09144	-126.40362	-126.86089	-126.86089	-126.86089
ϵ_{33-26}	-87.69123	-87.88959	-88.00419	-88.00418	-88.00418
ϵ_{37-40}	-73.27801	-72.88107	-72.93437	-72.93437	-72.93437
ϵ_{41-46}	-66.86798	-67.11111	-67.14079	-67.14078	-67.14078
ϵ_{47-52}	-47.78011	-47.45864	-47.45576	-47.45576	-47.45576
ϵ_{53-60}	-45.50042	-45.73773	-45.72233	-45.72233	-45.72233
...	...	...	...	...	...
ϵ_{110}	-1.16575	-1.17660	-1.17408	-1.17409	-1.17409
ϵ_{111}	-1.00557	-1.00535	-1.00795	-1.00795	-1.00795
ϵ_{112}	-1.00485	-1.00463	-1.00724	-1.00724	-1.00724
ϵ_{113}	-0.54122	-0.53307	-0.53604	-0.53603	-0.53603
ϵ_{114}	-0.53907	-0.53085	-0.53384	-0.53384	-0.53384
ϵ_{115}	-0.20929	-0.21028	-0.21007	-0.21007	-0.21007
ϵ_{116}	-0.19942	-0.20048	-0.20027	-0.20027	-0.20027
ϵ_{117}	-0.19101	-0.19215	-0.19194	-0.19194	-0.19194
ϵ_{118}	-0.18304	-0.18421	-0.18401	-0.18400	-0.18400

functional within a KS-DFT-based SCF approach. By contrast, to the best of our knowledge common PCE schemes such as the AMFI approach do – by construction – *not* allow to distinguish between 2eSO PCE corrections for the X2C Hamiltonian that either aim for an ensuing (uncorrelated) 2c HF or (correlated) KS-DFT-based many-electron SCF calculation. Bearing these subtle, yet crucial details in mind, the strikingly excellent numerical performance of our (e)amfX2C$_{DC}$ models wrt the ^{4}DC reference spinor energies as well as total energies which are illustrated in Table III not only underlines the outstanding numerical performance of our newly proposed PCE correction *ansätze* but is also in perfect agreement with our previous conclusions within the HF approach (*vide supra*). Moreover, the SO splittings Δ_X^{SO} of the (e)amfX2C$_{DC}$ and ^{4}DC cases match again exactly within significant digits for all the selected inner-core and outer-core atomic-like shells shown in Figure 1b. Notably, as indicated above, the (basis-set dependent) AMFI-based SO PCE corrections are SCF-model independent and, hence, strictly identical for both common use cases, *viz.* in an X2C-HF and X2C-KS-DFT approach. Consequently, AMFI does not include *a priori* any PCE corrections on the SO splitting originating from amf *two-electron correlation effects* which should primarily have an impact on the resulting splitting of the most strongly SO-split p shells. A close inspection of the left (HF) and right (DFT/PBE) panels of Figure 1 reveals that the deviations from the ^{4}DC reference for $\Delta_X^{SO}(X = 2p, 3p, 4p)$ are indeed systematically larger in the (correlated) DFT/PBE case.

c. On the importance of two-electron scalar-relativistic PCE corrections In the previous paragraphs, we discussed the performance of our newly proposed (e)amf PCE corrections for the X2C Hamiltonian in either a HF or KS-DFT framework with a particular focus on *relative* spinor energies of the superheavy diatomic molecule Og_2, that is, for example on the resulting SO splittings of inner- and outer-core atomic-like shells by comparison to the corresponding ^{4}DC reference data. In order to highlight the full potential of our (e)amf PCE models, let us recall that our 2ePCE correction models take into account both 2eSO *and* 2eSC correction terms. Whereas 2eSO PCE corrections are common to include in an (exact) two-component Hamiltonian framework for many-electron systems,[34,37,38,41] the inclusion of 2eSC-PCE correction terms is less so, despite their apparent significance to be illustrated in the following. To this end, we turn to a genuine spinfree SC framework by eliminating all spin-dependent terms from the parent ^{4}DC Hamiltonian by means of the Dirac relation.[33,92] Hence, results obtained on the basis of the SC-^{4}DC Hamiltonian will serve as references for the discussion of the numerical performance of various PCE-corrected SC-X2C Hamiltonian

Table IV: SCF total energy (E) and orbital energies of selected doubly-degenerate occupied orbitals (ϵ) for Og_2 as obtained from HF/`v2z` calculations within a scalar-relativistic (SC) four-component Dirac-Coulomb (^{4}DC) as well as a two-component Hamiltonian framework, including the new SC-(e)amfX2C$_{DC}$ models. All energies are given in Hartree.

	SC-1eX2C$_D$	SC-AMFIX2C$_D$	SC-amfX2C$_{DC}$	SC-eamfX2C$_{DC}$	SC-^{4}DC
E	-109086.48892	-109086.48892	-109171.75916	-109171.75916	-109171.75917
ϵ_{1-2}	-8263.96172	-8263.96172	-8291.15582	-8291.15582	-8291.15582
ϵ_{3-4}	-1738.62822	-1738.62822	-1743.94621	-1743.94621	-1743.94621
ϵ_{5-10}	-1263.67816	-1263.67816	-1264.70996	-1264.70996	-1264.70996
ϵ_{11-12}	-476.53515	-476.53515	-477.77497	-477.77497	-477.77497
ϵ_{13-18}	-350.21316	-350.21316	-350.49958	-350.49958	-350.49958
ϵ_{19-28}	-274.23599	-274.23599	-274.32251	-274.32250	-274.32250
ϵ_{29-30}	-142.64244	-142.64244	-142.98885	-142.98885	-142.98885
ϵ_{31-36}	-101.55738	-101.55738	-101.63035	-101.63035	-101.63035
ϵ_{37-46}	-72.82370	-72.82370	-72.83682	-72.83682	-72.83682
ϵ_{47-60}	-48.96807	-48.96807	-48.96163	-48.96163	-48.96163
...	...	...	...	...	...
ϵ_{110}	-1.61633	-1.61633	-1.61483	-1.61482	-1.61482
ϵ_{111}	-1.31132	-1.31132	-1.31593	-1.31593	-1.31593
ϵ_{112}	-1.31005	-1.31005	-1.31467	-1.31467	-1.31467
ϵ_{113}	-0.41445	-0.41445	-0.41435	-0.41435	-0.41435
ϵ_{114}	-0.39648	-0.39648	-0.39639	-0.39639	-0.39639
ϵ_{115}	-0.39648	-0.39648	-0.39639	-0.39639	-0.39639
ϵ_{116}	-0.38981	-0.38981	-0.38972	-0.38972	-0.38972
ϵ_{117}	-0.38981	-0.38981	-0.38972	-0.38972	-0.38972
ϵ_{118}	-0.37349	-0.37349	-0.37341	-0.37341	-0.37341

models. For the ease of comparison with the above spin-dependent data, we consider in Tables IV and V, respectively, in a spinfree *ansatz* the same superheavy diatomic molecule Og_2.

A close inspection of both tables first shows that the bare (no PCE corrections) SC-1eX2C$_D$ and the SC-AMFIX2C$_D$ Hamiltonians yield within either computational model, *viz.* HF and DFT/PBE, strictly matching numerical results. The reason is that with the elimination of any spin-dependent term from the (parent) 4c Hamiltonian, the AMFI PCE corrections simply become zero. Moreover, as could be expected, the largest 2eSC PCE corrections are encountered for the inner s shells (molecular spinors ϵ_{1-4} in Tables IV and V) with deviations for SC-1eX2C$_D$ ($\equiv$ SC-AMFIX2C$_D$) up to 27.2 Hartree in the HF and 35.3 Hartree in the DFT/PBE case compared to the SC-^{4}DC reference data. By moving to the outer-core and up to occupied molecular spinors close to the Fermi level, 2eSC PCEs start to fade significantly with absolute deviations for the HOMO and HOMO-1 amounting to less than 10^{-4} Hartree. By contrast, our SC-(e)amfX2C$_{DC}$ models provide an even higher numerical accuracy by at least one order of magnitude ($< 10^{-5}$) for *all* occupied molecular spinors summarized in Tables IV and V, that is ranging from the innermost s shells to the Fermi level. The latter findings therefore unequivocally illustrate that our atomic SC-(e)amfX2C$_{DC}$ PCE correction models are capable of efficiently correcting for 2ePCEs in a molecular framework. Consequently, this distinct asset of our (e)amfX2C models is a key ingredient for their above discussed numerical success in a spin-dependent Hamiltonian framework where 2eSC and 2eSO coupling contributions are both simultaneously at play and should not be considered on a different footing. In passing we further note that also in the present spinfree case the total SCF energies obtained within either our (e)amfX2C or a 4c Hamiltonian framework agree up to μ-Hartree accuracy, regardless of the underlying SCF *ansatz*.

2. Open-shell Te_2

In the previous Section IV A 1, we primarily focused on the numerical assessment of various 2ePCE corrections schemes for the X2C Hamiltonian in a many-electron context on the basis of the closed-shell superheavy diatomic molecule Og_2. In particular, we paid attention to the capability of various 2ePCE-corrected X2C models to provide matching molecular spinor energies by comparison to four-component reference data. In the chemistry of (molecular compounds of) heavy and superheavy elements, one frequently has to cope with partially occupied electronic shells due to the possibility of unfilled s, p, d and/or f electronic shells. In order to showcase the versatility of our (e)amf PCE corrections for the X2C Hamiltonian also in such a context, we consider in the following the open-shell molecule Te_2.

Table V: SCF total energy (E) and spinor energies of selected doubly-degenerate occupied spinors (ϵ) for Og_2 as obtained from DFT/PBE/**v2z** calculations within a scalar-relativistic (SC) four-component Dirac-Coulomb (^{4}DC) as well as a two-component Hamiltonian framework, including the new SC-(e)amfX2C$_{DC}$ models. All energies are given in Hartree.

	SC-1eX2C$_D$	SC-AMFIX2C$_D$	SC-amfX2C$_{DC}$	SC-eamfX2C$_{DC}$	SC-^{4}DC
E	-109137.69723	-109137.69723	-109230.56534	-109230.56535	-109230.56535
ϵ_{1-2}	-8210.62133	-8210.62133	-8245.93922	-8245.93921	-8245.93922
ϵ_{3-4}	-1719.07635	-1719.07635	-1725.22140	-1725.22140	-1725.22140
ϵ_{5-10}	-1248.58616	-1248.58616	-1251.03614	-1251.03614	-1251.03614
ϵ_{11-12}	-466.81628	-466.81628	-468.19109	-468.19109	-468.19109
ϵ_{13-18}	-342.38739	-342.38739	-342.98598	-342.98598	-342.98598
ϵ_{19-28}	-267.99753	-267.99753	-268.22450	-268.22450	-268.22450
ϵ_{29-30}	-137.50875	-137.50875	-137.87818	-137.87817	-137.87817
ϵ_{31-36}	-97.30211	-97.30211	-97.45128	-97.45127	-97.45127
ϵ_{37-46}	-69.59460	-69.59460	-69.63417	-69.63415	-69.63415
ϵ_{47-60}	-46.68630	-46.68630	-46.68201	-46.68200	-46.68200
...	...	...	...	...	...
ϵ_{110}	-1.29793	-1.29793	-1.29619	-1.29618	-1.29618
ϵ_{111}	-1.01944	-1.01944	-1.02282	-1.02281	-1.02281
ϵ_{112}	-1.01877	-1.01877	-1.02215	-1.02215	-1.02215
ϵ_{113}	-0.28186	-0.28186	-0.28190	-0.28190	-0.28190
ϵ_{114}	-0.26843	-0.26843	-0.26851	-0.26850	-0.26850
ϵ_{115}	-0.26843	-0.26843	-0.26851	-0.26850	-0.26850
ϵ_{116}	-0.26331	-0.26331	-0.26339	-0.26339	-0.26339
ϵ_{117}	-0.26331	-0.26331	-0.26339	-0.26339	-0.26339
ϵ_{118}	-0.25140	-0.25140	-0.25151	-0.25150	-0.25150

The latter system is a heavy homologue of O_2 and for this reason best characterized by a valence electronic structure that can be written in shorthand as $\pi_u^4\pi_g^{*,2}$ (assuming an approximate yet more familiar spin-orbit-free notation of the molecular spinors). For a further, detailed discussion of the electronic structure of the homonuclear diatomic systems of group 16 ranging from O_2 to Po_2, we refer the reader, for example, to Ref. 83. As shown in the latter, the molecular bonding (π_u) and antibonding (π_g^*) combinations predominantly originate from the atomic p valence shells of each Te atom. Hence, their actual description will be a sensitive measure of an appropriate account of both SC effects and SO coupling. To this end, we will not only consider spin-same-orbit but also spin-other-orbit interaction effects where the latter requires the inclusion of the 2e Gaunt term in the many-body Dirac Hamiltonian.[3,93]

In Table VI, we start our assessment of molecular spinor energies of Te_2 obtained by means of AOC-HF calculations by comparing first data based on various 2ePCE corrections schemes for the X2C Hamiltonian to 4c Dirac-Coulomb Hamiltonian reference values. Notably, for the (closed) core electronic shells we observe for all 2c Hamiltonian schemes similar trends as was the case for Og_2 – with a reference-matching accuracy of our (e)amfX2C models better than 5×10^{-5} Hartree – which underlines the numerical superiority of our newly proposed PCE correction schemes also in an open-shell case. Moving next to the lower end of Table VI, that is the (partially) occupied valence π (ϵ_{50-51}) and π^* (ϵ_{52-53}) shells, we first note that employing a bare 1eX2C$_D$ Hamiltonian does not suffice to achieve sub-mHartree accuraccy in the description of the spin-orbit-split m_j components of the $\pi^{(*)}$ shells, in particular so for the $\pi^*_{1/2} - \pi^*_{3/2}$ shells (ϵ_{52} and ϵ_{53} in Table VI, respectively). By contrast, – as opposed to the superheavy diatomic Og_2 – for the heavy Te_2 diatomic system the AMFIX2C$_D$ Hamiltonian yields results for the valence shells on par with the (e)amfX2C$_{DC}$ Hamiltonian both of which are in turn in excellent agreement with the ^{4}DC reference.

We note in passing that the excellent agreement in *absolute* values between AMFIX2C$_D$-based data (encompassing spin-same and spin-other-orbit PCE corrections) and the ^{4}DCG reference deteriorates not only for the inner-core shells but also for the valence $\pi^{(*)}$ manifolds as shown in Table VIII. More importantly, though, *relative* energy differences are, to a large extent, preserved in the valence shells of Te_2 which suggests that the AMFIX2C$_D$ model could still be a viable option for a 2c Hamiltonian framework when aiming for a study of valence-shell dominated molecular properties. Albeit the reasonable relative energy differences in the latter case, to achieve simultaneously both accurate absolute and relative molecular spinor energies with respect to the ^{4}DC as well as ^{4}DCG reference data necessitates to resort to our (e)amfX2C Hamiltonian models. As can be inferred from Tables VI and VIII, both our amf 2ePCE correction models display for *all* electronic shells a numerical accuracy within at least a few 10^{-5} Hartree (or better) in comparison to the respective 4c reference.

Table VI: SCF total energy (E) and spinor energies (ϵ) of the doubly-degenerate occupied and (partially occupied) open-shell spinors for Te_2 as obtained from AOC/HF/`v2z` calculations within a four-component Dirac-Coulomb (^{4}DC) as well as a two-component Hamiltonian framework, including the new (e)amfX2C$_{DC}$ models. All energies are given in Hartree.

	1eX2C$_D$	AMFIX2C$_D$	amfX2C$_{DC}$	eamfX2C$_{DC}$	^{4}DC
E	-13584.54193	-13584.34021	-13587.74121	-13587.74119	-13587.74174
ϵ_{1-2}	-1174.97331	-1174.97784	-1176.01576	-1176.01576	-1176.01572
ϵ_{3-4}	-183.75495	-183.75645	-183.87640	-183.87640	-183.87640
ϵ_{5-6}	-172.03541	-171.69323	-171.76385	-171.76385	-171.76385
ϵ_{7-8}	-161.41635	-161.57069	-161.63731	-161.63730	-161.63731
ϵ_{9-10}	-161.41620	-161.57054	-161.63716	-161.63716	-161.63716
ϵ_{11-12}	-38.10899	-38.10952	-38.13087	-38.13086	-38.13086
ϵ_{13-14}	-33.17192	-33.10276	-33.11302	-33.11302	-33.11302
ϵ_{15-16}	-31.13206	-31.16370	-31.17336	-31.17335	-31.17335
ϵ_{17-18}	-31.13092	-31.16256	-31.17222	-31.17222	-31.17222
ϵ_{19-20}	-22.49155	-22.43146	-22.43228	-22.43228	-22.43228
ϵ_{21-22}	-22.48993	-22.42984	-22.43065	-22.43065	-22.43065
ϵ_{23-24}	-21.99104	-22.03063	-22.03248	-22.03247	-22.03247
ϵ_{25-26}	-21.99031	-22.02990	-22.03175	-22.03174	-22.03174
ϵ_{27-28}	-21.98893	-22.02852	-22.03037	-22.03038	-22.03038
...	...	...	...	...	...
ϵ_{47}	-0.86560	-0.86565	-0.86590	-0.86590	-0.86590
ϵ_{48}	-0.70308	-0.70312	-0.70348	-0.70347	-0.70347
ϵ_{49}	-0.41423	-0.41390	-0.41389	-0.41389	-0.41389
ϵ_{50}	-0.36588	-0.36517	-0.36514	-0.36513	-0.36513
ϵ_{51}	-0.34337	-0.34389	-0.34386	-0.34387	-0.34387
ϵ_{52}	-0.26021	-0.25990	-0.25990	-0.25990	-0.25990
ϵ_{53}	-0.23943	-0.24003	-0.24003	-0.24003	-0.24003

3. Methane – the ultrarelativistic case

In contrast to the previous molecular examples, methane (CH_4) consists of a "heavy" carbon atom C and four "light" hydrogen atoms H. Particularly, since hydrogen is a *one*-electron system, it will not give rise to atomic *two*-electron PCE-correction terms. Hence, any genuine *atomic*-mean-field-based PCE-corrected 2c Hamiltonian such as AMFIX2C or amfX2C will, by construction, not include any "light"-atom PCE corrections. By contrast, our extended amfX2C approach allows us to eliminate this apparent shortcoming because, as detailed in Section II C and outlined in lines 14-23 of Alg. 2, all PCE-correction terms for HF and DFT, respectively, are derived in *molecular* basis on the basis of molecular densities, $\boldsymbol{D}^{4c}_{\oplus}$ and $\boldsymbol{D}^{2c}_{\oplus}$, built from a superposition of atomic input densities. Consequently, the essential molecular densities include atomic contributions regardless of the actual atom type, *viz.* "light" (one-electron) and "heavy" (many-electron) atom contribute on an equal footing.

Bearing the latter in mind, the total SCF energies as well as spinor energies compiled in Table IX for an ultrarelativistic CH_4 with the speed of light c scaled down by a factor 10 confirm the unique numerical performance of the eamfX2C$_{DC}$ Hamiltonian model in comparison to the ^{4}DC reference data. Only in the eamfX2C$_{DC}$ case (column 4, Table IX), we find that not only the total energy E agrees to better than mHartree accuracy but also the spinor energies exhibit consistent numerical accuracy for the innermost non-bonding core C 1s as well as the bonding, valence C-H spinors. Notably, the amfX2C$_{DC}$ as well as the AMFIX2C$_D$ models feature an inconsistent numerical performance wrt both quantities: amfX2C$_{DC}$ yields a total energy E and spinor energies for the (carbon-centered) inner core spinors ϵ_1 and ϵ_2, respectively, of the ultrarelativistic CH_4 which are in close agreement with the ^{4}DC reference. It shows, however, larger deviations for the valence spinors (ϵ_{3-5}) whereas the opposite conclusions apply to the AMFIX2C$_D$-based data. In the latter case, we ascribe the seemingly good performance of the AMFIX2C$_D$ Hamiltonian with errors less than a mHartree in comparison to the ^{4}DC reference to a fortuitous error cancellation since the amf based AMFI PCE correction scheme cannot take into account any 2e picture-change corrections that involve contributions from the atomic hydrogen centers.

Table VII: SCF total energy (E) and spinor energies (ϵ) of occupied spinors for Te_2 as obtained from Kramers-unrestricted HF/v2z calculations within a four-component Dirac-Coulomb (^{4}DC) as well as a two-component Hamiltonian framework, including the new (e)amfX2C$_{DC}$ models. All energies are given in Hartree.

	1eX2C$_D$	amfX2C$_{DC}$	eamfX2C$_{DC}$	^{4}DC
E	-13584.66007	-13587.85859	-13587.85862	-13587.85937
ϵ_{1-2}	-1174.97217	-1176.01450	-1176.01450	-1176.01466
	-1174.96988	-1176.01219	-1176.01219	-1176.01243
ϵ_{3-4}	-183.75281	-183.87441	-183.87441	-183.87442
	-183.75200	-183.87360	-183.87360	-183.87362
ϵ_{5-6}	-172.03333	-171.76193	-171.76192	-171.76192
	-172.03307	-171.76167	-171.76166	-171.76167
ϵ_{7-8}	-161.41472	-161.63582	-161.63581	-161.63582
	-161.41462	-161.63572	-161.63571	-161.63572
ϵ_{9-10}	-161.41262	-161.63373	-161.63373	-161.63376
	-161.41259	-161.63370	-161.63370	-161.63373
ϵ_{11-12}	-38.10749	-38.12953	-38.12953	-38.12953
	-38.10495	-38.12698	-38.12698	-38.12698
ϵ_{13-14}	-33.16988	-33.11113	-33.11113	-33.11113
	-33.16937	-33.11064	-33.11063	-33.11064
ϵ_{15-16}	-31.13053	-31.17199	-31.17199	-31.17199
	-31.13050	-31.17195	-31.17195	-31.17195
ϵ_{17-18}	-31.12656	-31.16803	-31.16803	-31.16804
	-31.12652	-31.16800	-31.16800	-31.16800
ϵ_{19-20}	-22.48891	-22.42980	-22.42980	-22.42980
	-22.48870	-22.42958	-22.42958	-22.42958
ϵ_{21-22}	-22.48751	-22.42839	-22.42838	-22.42839
	-22.48748	-22.42836	-22.42835	-22.42836
ϵ_{23-24}	-21.98841	-22.03001	-22.03000	-22.03001
	-21.98819	-22.02979	-22.02978	-22.02978
...	...	...	...	...
ϵ_{99}	-0.41895	-0.41881	-0.41881	-0.41880
ϵ_{100}	-0.39775	-0.39742	-0.39742	-0.39742
ϵ_{101}	-0.32364	-0.32379	-0.32379	-0.32379
ϵ_{102}	-0.32115	-0.32151	-0.32151	-0.32151
ϵ_{103}	-0.31781	-0.31769	-0.31769	-0.31769
ϵ_{104}	-0.31521	-0.31527	-0.31528	-0.31528

B. Contact densities of copernicium fluorides CnF$_n$

In this section, we assess the accuracy of calculating absolute contact densities as well as the potential to provide reliable relative contact-density shifts computed within PCE-corrected X2C Hamiltonian models by comparing to parent 4c reference data. While absolute contact densities are dominated by contributions of the inner s-shells, and to a lesser extent the innermost $p_{1/2}$-shells, of the respective nuclear center of interest, contact-density shifts particularly probe subtle differences of the valence electronic structure and, likewise, polarization of the inner electronic shells both of which originate from the chemical bonding between a reference atom, here the Cn atom, and ligand atoms (or molecules), as, for example, the n fluorine atoms in the CnF$_n$ compounds studied in the present work. The optimized structures of the CnF$_n$ ($n = 2, 4, 6$) compounds along with the corresponding spatial symmetries are shown in Table X. Considering the limited basis-set size and point-nucleus approximation in the present work, our optimized Cn-F bond lengths r_{Cn-F} compare reasonably with corresponding benchmark data from a very recent work by Hu and Zou[85] who reported X2C/PBE0-optimized bond lengths r_{Cn-F} of 1.920, 1.927 and 1.933 Å with an increasing number n of fluorine ligand atoms.

Table XI summarizes the calculated absolute contact densities as well as density shifts in a spin-dependent (upper panel) and scalar-relativistic (spinfree, lower panel) framework. As can be seen there, by construction, we find for the bare Cn atom a perfect match for the absolute contact density at the Cn nucleus between our (e)amfX2C$_{DC}$ PCE-corrected 2c calculations (Table XI, entries 4 and 5) and the corresponding 4c reference, irrespective of the inclusion of spin-dependent terms. By contrast, discarding any 2ePCE corrections (1eX2C$_D$, entry 2) or including only first-order SO mean-field PCE corrections (AMFIX2C$_D$, entry 3) leads to a considerable underestimation of the total contact density. Interestingly, in the AMFIX2C$_D$ case, the total contact density is even smaller than in the

Table VIII: SCF total energy (E) and spinor energies (ϵ) of the doubly-degenerate occupied and open-shell spinors for Te_2 as obtained from AOC/HF/`v2z` calculations within a four-component Dirac-Coulomb-Gaunt (^{4}DCG) as well as a two-component Hamiltonian framework, including the new (e)amfX2C$_{\mathrm{DCG}}$ models. All energies are given in Hartree.

	1eX2C$_{\mathrm{D}}$	AMFIX2C$_{\mathrm{D}}$	amfX2C$_{\mathrm{DCG}}$	eamfX2C$_{\mathrm{DCG}}$	^{4}DCG
E	-13584.54193	-13584.25457	-13576.46087	-13576.46083	-13576.45740
ϵ_{1-2}	-1174.97331	-1174.98060	-1173.19796	-1173.19796	-1173.19789
ϵ_{3-4}	-183.75495	-183.75737	-183.61571	-183.61571	-183.61570
ϵ_{5-6}	-172.03541	-171.61303	-171.29409	-171.29409	-171.29408
ϵ_{7-8}	-161.41635	-161.60382	-161.30279	-161.30279	-161.30280
ϵ_{9-10}	-161.41620	-161.60366	-161.30263	-161.30264	-161.30263
ϵ_{11-12}	-38.10899	-38.10982	-38.09468	-38.09468	-38.09468
ϵ_{13-14}	-33.17192	-33.08683	-33.04133	-33.04133	-33.04133
ϵ_{15-16}	-31.13206	-31.17031	-31.12709	-31.12708	-31.12709
ϵ_{17-18}	-31.13092	-31.16916	-31.12594	-31.12595	-31.12595
ϵ_{19-20}	-22.49155	-22.42520	-22.41206	-22.41206	-22.41206
ϵ_{21-22}	-22.48993	-22.42358	-22.41044	-22.41044	-22.41044
ϵ_{23-24}	-21.99104	-22.03503	-22.02348	-22.02347	-22.02347
ϵ_{25-26}	-21.99031	-22.03430	-22.02275	-22.02275	-22.02275
ϵ_{27-28}	-21.98893	-22.03293	-22.02138	-22.02139	-22.02139
...	...	...	...	...	...
ϵ_{47}	-0.86560	-0.86567	-0.86583	-0.86582	-0.86582
ϵ_{48}	-0.70308	-0.70313	-0.70323	-0.70322	-0.70322
ϵ_{49}	-0.41423	-0.41382	-0.41360	-0.41359	-0.41360
ϵ_{50}	-0.36588	-0.36501	-0.36480	-0.36479	-0.36479
ϵ_{51}	-0.34337	-0.34400	-0.34382	-0.34383	-0.34383
ϵ_{52}	-0.26021	-0.25983	-0.25952	-0.25953	-0.25953
ϵ_{53}	-0.23943	-0.24016	-0.23987	-0.23987	-0.23987

Table IX: SCF total energy (E) and spinor energies (ϵ) of the doubly-degenerate occupied spinors for CH_4 as obtained from DFT/PBE/`v2z` calculations within a four-component Dirac-Coulomb (^{4}DC) as well as a two-component Hamiltonian framework, including the new (e)amfX2C$_{\mathrm{DC}}$ models. All energies are given in Hartree. The speed of light c was reduced by a factor 10.

	1eX2C$_{\mathrm{D}}$	AMFIX2C$_{\mathrm{D}}$	amfX2C$_{\mathrm{DC}}$	eamfX2C$_{\mathrm{DC}}$	^{4}DC
E	−42.142 20	−42.140 39	−42.264 69	−42.257 74	−42.258 50
ϵ_1	−10.222 06	−10.224 01	−10.361 54	−10.360 28	−10.357 94
ϵ_2	−0.659 39	−0.659 66	−0.662 88	−0.662 69	−0.662 74
ϵ_3	−0.357 05	−0.352 88	−0.356 49	−0.352 91	−0.352 90
ϵ_{4-5}	−0.333 13	−0.335 03	−0.332 82	−0.335 27	−0.335 44

1eX2C$_{\mathrm{D}}$ case and, consequently, in even stronger disagreement with the 4c reference. Moving next to the difluoride compound, the conclusions surprisingly seem to shift. While all 2c models correctly reproduce the trend of a decrease in the contact density at the Cn nucleus, AMFIX2C$_{\mathrm{D}}$ (923.43 e/a_0^3, spinfree: 1225.51 e/a_0^3) now exhibits the best agreement for the contact density shift with the (sc-)^{4}DC reference of 922.84 e/a_0^3 (1226.40 e/a_0^3). Considering the remaining tetra- and hexafluoride compounds in Table XI, the agreement of AMFIX2C$_{\mathrm{D}}$ for $\Delta\rho$ with the 4ct references considerably worsens with an increasing number of fluorine ligands. This leads us to conclude that the almost perfect

Table X: Four-component DFT/PBE0-optimized structures of CnF_n ($n = 2, 4, 6$) compounds. For computational details, see text. All internuclear distances $r_{\mathrm{Cn-F}}$ are given in Å.

molecule	$r_{\mathrm{Cn-F}}$	double group symmetry
CnF_2	1.9374	$D^*_{\infty h}$
CnF_4	1.9418	C^*_{4h}
CnF_6	1.9477	O^*_h

match in $\Delta\rho$ observed for CnF_2 is likely due to a fortuitous error cancellation.

What about the (e)amfX2C models? For CnF_2, a decomposition of the total contact density at the Cn nucleus in terms of molecular spinor contributions reveals that calculations based on the (e)amfX2C$_{\mathrm{DC}}$ Hamiltonian predict in the spin-dependent case – similar conclusions hold for the spinfree case – a major contribution of the Cn $1s$ shell (*vide supra*) of -43605705.12 e/a_0^3 (-43605705.33 e/a_0^3) in contrast to the 4c value of -43605699.65 e/a_0^3. Hence, recalling the exact numerical match within significant digits for the bare Cn atom (see Table XI, first row), the major source for the difference in the total $\Delta\rho$ for CnF_2 predominantly traces back to a $\Delta\rho_{1s} \approx 5.5\ e/a_0^3$ between our 2c (e)amfX2C$_{\mathrm{DC}}$ and the ^{4}DC data. Moreover, it is precisely for this innermost electronic shell that the molecular spinor energies ϵ_{1s} exhibit deviations between (e)amfX2C and ^{4}DC on the order of $+3 \times 10^{-4}$ Hartree. In detail, we obtain in both 2c cases $\epsilon_{1s}^{\mathrm{amfX2C_{DC}}} = -7117.03293$ Hartree and $\epsilon_{1s}^{\mathrm{eamfX2C_{DC}}} = -7117.03294$ Hartree, respectively, underlining the obvious close relationship of the two approaches, which have to be compared with $\epsilon_{1s}^{^4\mathrm{DC}} = -7117.03260$ Hartree. Despite the slightly increasing discrepancies in $\Delta\rho$ observed for the remaining polyatomic fluoride compounds of Cn listed in Table XI which can be explained along the same lines as for the difluoride CnF_2 compound, our (e)amfX2C models yet perform best in a systematic fashion with respect to the four-component references. Notably, these encouraging findings hold for both common use cases, with the inclusion of SO interaction and in a genuine spinfree approach. In summary, probing the density at a heavy nucleus constitutes an excellent measure of the importance of 2e interaction contributions and, hence, allows us to uniquely reveal even subtle shortcomings of distinct 2ePCE correction models within the X2C Hamiltonian framework by comparing to the corresponding full 4c reference data.

C. X-ray core ionization energies

Finally, we compare the performance and reliability of the 1eX2C, AMFIX2C as well as (e)amfX2C 2c Hamiltonian models for the calculation of X-ray core ionization energies by comparing to corresponding mmfX2C reference values. With the advent and general accessibility of new, powerful X-ray radiation sources such as free-electron lasers[94] (see for example Ref. 95 for an overview of available facilities), experimental X-ray spectroscopies have witnessed in the past decade a continuous, rapid advance and enhanced applicability to study not only the electronic structure but also the dynamics of molecules and materials.[96–98] In order to keep pace with the experimental progress and being able to provide a much welcomed highly accurate theoretical support, computational X-ray spectroscopy has experienced tremendous progress in recent years.[99] Here, a genuine inclusion of relativistic effects is nothing but a basic requirement since the inner-core shells are most prone to quantitative changes due to relativity. For example, while K-edge X-ray spectroscopy probes the chemical nature of the $1s_{1/2}$ shell of a given center and, hence, necessitates in particular a proper account of SC contributions, studying the L- and M-edge of (late) transition-metal, p-block and, perhaps most importantly, f-elements[100], whose fine-structure is dominated by the SO splitting of the $2p$- and $3p$- and $3d$-shells, respectively, requires a suitable framework to efficiently take into account the SO interaction. The latter two requirements are easily met in either a (exact) 2c or full 4c framework that sets out from a many-particle Dirac-Coulomb(-Gaunt/-Breit) Hamiltonian. For further details and recent advances of genuine relativistic quantum-chemical X-ray spectrocsopy approaches that illustrate in a striking fashion the potential of such ansätze, we refer the reader, for example, to Refs. 89,101–104.

Considering common applications in X-ray spectroscopy, we highlight in Tables XII and XIII the importance of 2ePCE corrections to the X2C Hamiltonian which we may anticipate, based on all findings discussed in the previous sections (*vide supra*), to be most pronounced for the K- up to M-edges of heavy- and superheavy nuclei. Starting with the EOM-CCSD core-ionization potentials of the heavy p-block anion At^- compiled in Table XII, we note that the K-edge ionisation potentials for within the 1eX2C$_{\mathrm{D}}$ and AMFIX2CD Hamiltonian frameworks deviate more than 5 Hartree (sic!) from the mmfX2C$_{\mathrm{DC}}$ reference. Concerning the use of the latter, it was shown in Ref. 89 that making use of this 2c Hamiltonian scheme yields ionization potentials which are virtually indistinguishable from the parent ^{4}DC data and this is indeed confirmed by the present calculations. Moving to our (e)amfX2C PCE-corrected Hamiltonian framework, we observe an agreement with the mmfX2C$_{\mathrm{DC}}$ data of sub-mHartree accuracy not only for the K- but also for the L_1 as well as $L_{2,3}$ edges. The resulting deviation of 27 cm^{-1} from the reference data for the SO-splitting $\Delta^{\mathrm{SO}}_{\mathrm{L-edge}}$ (5th row, Table XII), that ultimately governs the fine-structure of the $L_{2,3}$ edges, approaches almost *spectroscopic* accuracy of 1 cm^{-1}[105]. By contrast, the error for $\Delta^{\mathrm{SO}}_{\mathrm{L-edge}}$ in the case of employing, for example, the hitherto popular AMFIX2C$_{\mathrm{D}}$ Hamiltonian is as large as 21600 cm^{-1} (corresponding to an error that is 60 times (sic!) larger than the error bar for *chemical* accuracy).

Table XIII compiles core-ionization potential data for two representative molecular $5d$- (upper panel) and $6d$ (lower panel) complexes as obtained from EOM-CCSD calculations. As was the case for the At^- anion, we consider the numerical performance of different *atomic* mean-field 2ePCE-correction schemes for the X2C Hamiltonian by comparing to results calculated within a *molecular* mean-field 2c framework (Table XIII, entry 6). In passing we note

Table XI: Contact densities ρ and contact density shifts $\Delta\rho$ evaluated at the Cn nucleus for the Cn atom and different Cn fluoride compounds. All data was obtained from scalar-relativistic+spin-orbit (upper panel) and scalar-relativistic-only spinfree (lower panel) HF wave functions. For the two-component X2C Hamiltonian different two-electron picture-change effect corrections were employed, including the new (e)amfX2C$_{\mathrm{DC}}$ models. All densities are given in e/a_0^3.

compound	1eX2C$_{\mathrm{D}}$	AMFIX2C$_{\mathrm{D}}$	amfX2C$_{\mathrm{DC}}$	eamfX2C$_{\mathrm{DC}}$	^{4}DC
Cn	−58 697 556.08	−58 661 390.26	−58 977 494.39	−58 977 494.39	−58 977 494.39
CnF_2	−58 696 660.51	−58 660 466.83	−58 976 578.21	−58 976 577.94	−58 976 571.54
CnF_4	−58 695 900.03	−58 659 721.50	−58 975 824.80	−58 975 823.87	−58 975 812.06
CnF_6	−58 695 683.21	−58 659 514.86	−58 975 609.89	−58 975 608.50	−58 975 593.75
$\Delta\rho_{(CnF_2-Cn)}$	895.57	923.43	916.18	916.45	922.84
$\Delta\rho_{(CnF_4-Cn)}$	1656.05	1668.76	1669.58	1670.52	1682.33
$\Delta\rho_{(CnF_6-Cn)}$	1872.88	1875.40	1884.50	1885.89	1900.64
			spinfree		
Cn	−56 251 080.53	−56 251 080.53	−56 571 626.66	−56 571 626.66	−56 571 626.66
CnF_2	−56 249 855.02	−56 249 855.02	−56 570 406.42	−56 570 405.90	−56 570 400.26
CnF_4	−56 249 040.54	−56 249 040.54	−56 569 579.69	−56 569 578.93	−56 569 569.39
CnF_6	−56 248 766.28	−56 248 766.28	−56 569 295.28	−56 569 294.35	−56 569 283.33
$\Delta\rho_{(CnF_2-Cn)}$	1225.51	1225.51	1219.24	1220.76	1226.40
$\Delta\rho_{(CnF_4-Cn)}$	2039.99	2039.99	2046.97	2047.73	2057.27
$\Delta\rho_{(CnF_6-Cn)}$	2314.25	2314.25	2331.38	2332.31	2343.33

Table XII: EOM-CCSD/`dyall.acv3z` core-ionization energies of the At^- anion obtained within a two-component Hamiltonian framework employing different corrections for two-electron picture-change effects. Note, that for At^- amfX2C$_{DC}$ and eamfX2C$_{DC}$ yield identical results. All energies are given in Hartree.

Ionization	1eX2C$_D$	AMFIX2C$_D$	amfX2C$_{DC}$	amfX2C$^a_{DC}$	mmfX2C$_{DC}$ [b]
K-edge	3532.8949	3532.9393	3538.2640	3538.2642	3538.2639
L_1-edge	644.5913	644.6059	645.4290	645.4290	645.4290
L_2-edge	620.8625	618.7619	619.2730	619.2730	619.2728
L_3-edge	522.5137	523.2968	523.7092	523.7092	523.7092
Δ^{SO}_L	98.3488	95.4651	95.5638	95.5638	95.5636

[a] amf corrections calculated for a neutral At atom.
[b] mmfX2C$_{DC}$ $\equiv$ ^{2}DC^m values taken from Ref. 89.

Table XIII: EOM-CCSD/`v2z` core-ionization energies of the molecular compounds $[Au(Cl)_4]^-$ and CnF_6 obtained within a two-component Hamiltonian framework employing different corrections for two-electron picture-change effects, including the new (e)amfX2C$_{DC}$ models. All energies are given in Hartree.

Ionization	1eX2C$_D$	AMFIX2C$_D$	amfX2C$_{DC}$	eamfX2C$_{DC}$	mmfX2C$_{DC}$	^{4}DC
			$[AuCl_4]^-$			
K-edge	2982.8305	n/a	2986.9702	2986.9702	2986.9702	2986.9705
L_1-edge	531.1267	n/a	531.7386	531.7387	531.7386	531.7387
L_2-edge	509.7823	n/a	508.5810	508.5810	508.5809	508.5808
L_3-edge	440.0794	n/a	441.0060	441.0061	441.0060	441.0064
	440.0792	n/a	441.0058	441.0058	441.0058	441.0061
M_4-edge	85.6431	n/a	85.3486	85.3487	85.3486	85.3485
	85.6414	n/a	85.3471	85.3471	85.3471	85.3470
M_5-edge	81.9117	n/a	82.1323	82.1323	82.1322	82.1325
	81.9097	n/a	82.1302	82.1303	82.1302	82.1305
	81.9082	n/a	82.1290	82.1290	82.1290	82.1292
[a] Δ^{SO}_{L-edge}	69.7030	n/a	67.5751	67.5751	67.5750	67.5745
$\Delta\Delta^{SO}_{L-edge}$	2.1280	n/a	0.0001	0.0001	0	-
			CnF_6			
K-edge	7098.8642	7099.0856	7116.4597	7116.4597	7116.4590	7116.4585
L_1-edge	1450.8351	1450.9066	1454.3983	1454.3984	1454.3979	1454.3983
L_2-edge	1412.3308	1404.9511	1406.9201	1406.9201	1406.9198	1406.9194
L_3-edge	1003.1544	1005.1986	1006.4395	1006.4396	1006.4393	1006.4401
Δ^{SO}_{L-edge}	409.1763	399.7525	400.4806	400.4806	400.4804	400.4793
$\Delta\Delta^{SO}_{L-edge}$	8.6959	−0.7279	0.0002	0.0002	0	-

[a] calculated as $\Delta^{SO}(L_2\text{-}\bar{L}_3)$ using an arithmetic mean value for the L_3-edge.

that for the [Au]-complex (upper panel of Table XIII), we were not able to obtain a converged SCF solution for Au within the external SCF program RELSCF[106] that constitutes the basis for the AMFI module within DIRAC, and this is unfortunately a recurring problem. Considering first the full neglect of 2ePCE corrections within the 1eX2C$_D$ framework (Table XIII, entry 2), a similar picture emerges in both molecular cases as in the single-ion case. The absolute deviations for the ionization potentials of all K- to M-edges are substantial. Moreover, the same conclusions hold for relative deviations, exemplified by the SO-splittings Δ^{SO}_{L-edge} of the L-edge. Hence, these findings unequivocally demonstrate also in the context of X-ray spectroscopic quantities that 2ePCEs are substantial when probing molecular properties of the inner-core shells. Interestingly, though, the ligand-field induced splittings of the $M_{4,5}$-edges in the case of the [Au]-complex can be correctly reproduced within the 1eX2C$_D$ Hamiltonian framework. As can be seen for the CnF_2 complex, the inclusion of first-order mean-field SO PCE corrections (entry 3, Table XIII) within the AMFIX2C$_D$ Hamiltonian leads to a reduction of the error for Δ^{SO}_{L-edge} by one order of magnitude from $\Delta\Delta^{SO}_{L-edge} \approx +8.7$ Hartree (1eX2C$_D$) to $\Delta\Delta^{SO}_{L-edge} \approx -0.7$ Hartree. Still, the underlying absolute core-ionization potentials for the K- and L-edges exhibit a clear deviation ranging from approximately 1.2 Hartree for the L_3-edge to more than 17 Hartree for the K-edge in comparison to the mmfX2C$_{DC}$ data.

By contrast, the EOM-CCSD core-ionization potentials calculated within the (e)amfX2C$_{DC}$ Hamiltonian frameworks (entries 4 and 5 in Table XIII) stand out also in the molecular cases due to two distinct, appealing features, namely (i) the *absolute* ionization energies for all edges feature numerical values below sub-mHartree accuracy and

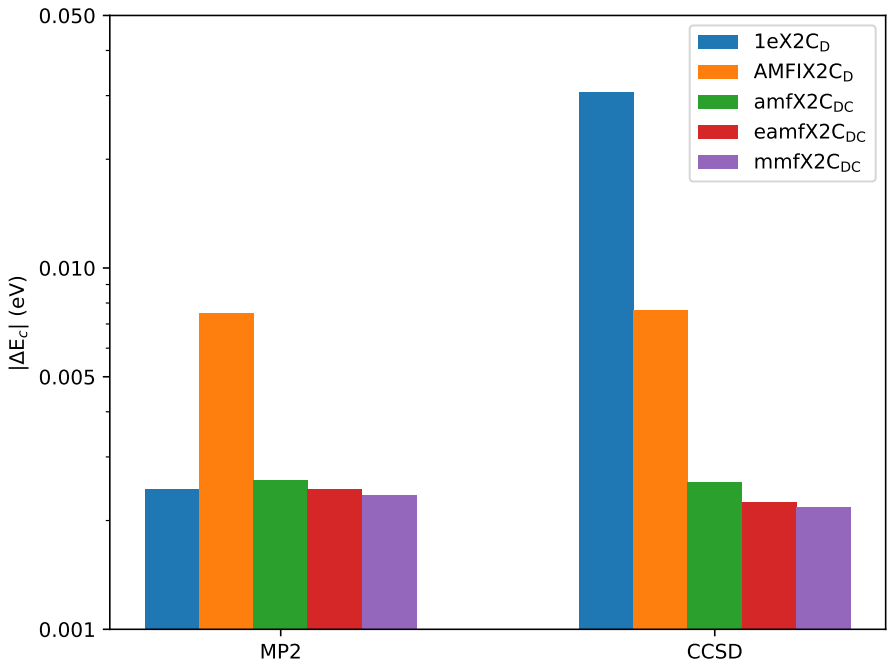

Figure 2: Absolute MP2 and CCSD correlation energies differences between ^{4}DC ($|\Delta E_c|$, in eV), for different Hamiltonian calculated for CnF_6 with the same computational setup as for the EOM-CCSD core-ionization energies. Note that the scale on the y-axis is logarithmic. Further computational details are given in the text.

(ii), as a result, this accuracy carries over to relative data such as the SO splitting of the $L_{2,3}$-edge and the ligand-field fine-structure splitting of the $M_{4,5}$-edges in the [Au]-complex. Hence, the atomic-meanfield (e)amfX2C Hamiltonian models can be regarded as a conceptually different alternative to the molecular mean-field ^{2}DC scheme by providing virtually the same numerical accuracy for core- and likewise valence molecular properties at a fraction of the computational effort. To stress the latter, we recall that the mmfX2C$_{\mathrm{DC}}$ approach requires to first find a converged *molecular* 4c SCF solution whereas our (e)amfX2C models are solely built on quantities obtained from *atomic* 4c SCF calculations. In the latter case, the SCF step is then carried out exclusively in a molecular 2c framework. Moreover, we note that, although the extended amfX2C Hamiltonian model requires the calculation of a single 2e Fock matrix $\boldsymbol{F}^{4c,2e}[\boldsymbol{D}^{4c}_{\oplus}]$ in a molecular four-component framework, an efficient density-matrix-based screening will significantly reduce the associated computational cost because of the sparsity of the atom-wise blocked 4c molecular density matrix $\boldsymbol{D}^{4c}_{\oplus}$.

Besides the calculation of core-binding energies within a 2c Hamiltonian framework taking into account various PCE correction models, we performed ^{4}DC-based EOM-CCSD calculation for the [Au]-complex as well as CnF_6 (Table XIII, entry 7). This enables us to further assess the influence of the Hamiltonian on the core ionizations, in particular inherent PCEs in the electron-electron interaction within a two-component X2C framework, regardless of an mmf or amf model to account for PCEs. As discussed in detail by Halbert *et al.* in Ref. 89 in the context of X-ray core binding energies, even for mmfX2C$_{\mathrm{DC}}$, which is based on the transformation into a 2c framework wrt a decoupling of the (converged) Fock matrix, leaving the 2e operator untransformed[32] necessarily introduces a PCE in the electron-electron interaction. Hence, the latter becomes most prominent for molecular properties that necessitate an accurate treatment of core-core and core-valence electron correlation such as X-ray core ionization potentials. Consequently, albeit our limited correlation treatment in the EOM-CCSD step (see Section III for further details), we already find small discrepancies for the K- and L-edge ionization energies between mmfX2C$_{\mathrm{DC}}$ and ^{4}DC on the order of 0.0025 eV and, similarly, for (e)amfX2C and ^{4}DC with differences up to 0.0035 eV in the case of CnF_6 while the deviations in the binding energies for the corresponding edges are smaller for the [Au]-complex because of the "lighter" Au central atom. As larger deviations – though still less than 0.01% of the total K-edge binding energy – had been observed in a corresponding comparison for astatine[89], we expect also for CnF_6 (and, similarly, for the [Au]-complex) a further increase of the deviations between ^{4}DC and (e)amfX2C$_{\mathrm{DC}}$ as well as mmfX2C$_{\mathrm{DC}}$ upon an improved electron-correlation treatment. In passing we note, though, the excellent performance of our extended amfX2C-based computational model (red error bars in Figure 2) with respect to the mmfX2C$_{\mathrm{DC}}$ model (purple error

Table XIV: EOM-CCSD/v2z core-ionization energies of CnF_6 including contributions from the two-electron Gaunt interaction obtained within a two-component Hamiltonian framework employing different corrections for two-electron picture-change effects, including the new (e)amfX2C$_{DCG}$ models. All energies are given in Hartree.

Ionization	1eX2C$_D$	AMFIX2C$_D$	amfX2C$_{DCG}$	eamfX2C$_{DCG}$	mmfX2C$_{DCG}$
K-edge	7098.8642	7099.2449	7076.5037	7076.5038	7076.5014
L_1-edge	1450.8351	1450.9603	1448.8009	1448.8010	1448.8003
L_2-edge	1412.3308	1402.7809	1397.8111	1397.8112	1397.8104
L_3-edge	1003.1544	1005.5519	1001.5403	1001.5404	1001.5405
Δ^{SO}_{L-edge}	409.1763	397.2290	396.2707	396.2707	396.2699
$\Delta\Delta^{SO}_{L-edge}$	12.9064	0.9591	0.0008	0.0008	0

bars in Figure 2) which are nearly identical for both MP2 and CCSD correlation energies even on a logarithmic scale in the case of CnF_6. By contrast, turning to 1eX2C$_D$ and AMFIX2C$_D$, respectively, we either find stark differences in the correlation errors between the MP2 and CCSD approaches (1eX2C$_D$) or, even within this limited correlation space, considerable errors in the correlation energies within AMFIX2C$_D$ by comparison to the ones obtained within a ^{4}DC framework. Taking together, these findings yet again underline the suitability and superiority of our amfX2C Hamiltonian models, in particular its extended variant, in the realm of an X2C framework for studying X-ray core binding energies of atoms and molecules comprising heavy and superheavy elements.

Finally, Table XIV compiles X-ray EOM-CSCD core binding energies of CnF_6 with the inclusion of the 2e Gaunt interaction. This allows us to highlight the significance of the Gaunt interaction (as part of the full Breit interaction) for an accurate description of the inner-core edges of (super-)heavy elements by comparing to the corresponding Coulomb-type-interaction only data shown above in Table XIII. Note that we do not have ^{4}DCG data at hand since the transformation of Gaunt-type AO integrals to MO basis is currently neither implemented in DIRAC nor in ReSpect. In addition, as discussed for Te_2 in Section IV A 2, 1eX2C$_D$ does not allow to take into account contributions from the Gaunt interaction and will not be considered further below.

In agreement to what has been concluded in Ref. 89 for astatide, we find for the (e)amfX2C$_{DCG}$ as well as mmfX2C$_{DCG}$ models (Table XIV, entries 4-6) a distinct effect arising from the Gaunt interaction. As a result, core-binding energies are substantially lowered by nearly 40 Hartree ($\approx$ 1.1 keV (!)) in case of the K- and by up to 9 Hartree for the L-edge, respectively. Moreover, we also observe a considerable decrease in the SO splitting of the $L_{2,3}$-edge Δ^{SO}_{L-edge} by approximately 115 eV which is very well captured ($\Delta\Delta^{SO}_{L-edge} \approx 0.02$ eV) by our (e)amfX2C$_{DCG}$ models in comparison to mmfX2C$_{DCG}$. The latter is in sharp contrast to the AMFIX2C$_D$ model (entry 3) which not only exhibits significant numerical differences in terms of absolute core-binding energies of more than 600 eV for the K-edge but also shows a quantitative error $\Delta\Delta^{SO}_{L-edge}$ of more than 25 eV for the $L_{2,3}$-edge fine-structure splitting.

V. CONCLUSIONS AND OUTLOOK

In this article we have presented the motivation for and derivation of two distinct, atomic-mean-field (amf) approaches to account on an equal footing for two-electron (2e) scalar-relativistic and spin-orbit picture-change effects (PCEs) arising within an exact-two-component (X2C) Hamiltonian framework. Both approaches, dubbed amfX2C and extended amf (eamfX2C) have been implemented independently in the Dirac[5] and ReSpect[6] programs. These implementations, which exploit – where available – atomic supersymmetry in the atomic self-consistent field steps,[5] open up for the calculation of two-electron picture-change effect corrections for all spin-dependent and spinfree four-component-based Hamiltonians available in the two quantum-chemical software packages.

Notably, we have shown that it is possible to uniquely tailor our amf 2ePCE corrections for the X2C Hamiltonian to the underlying classes of self-consistent field (SCF) *ansätze*, namely Hartree-Fock (HF) or density functional theory (DFT). Such a particular feature has, to the best of our knowledge, so far not been considered for any 2ePCE correction scheme in the literature. Moreover, by contrast to, for example, the recently proposed SOAMFX2C model[34] our new PCE correction schemes for the X2C Hamiltonian take into account both *spin-independent* – that is scalar-relativistic – and *spin-dependent* – that is spin-spin (arising from the Gaunt term[93]) as well as spin-orbit – contributions of the two-electron interaction. Perhaps most importantly, we also argue why the eamfX2C Hamiltonian can be employed in genuine two-component solid-state SCF calculations under consideration of periodic boundary conditions starting from an appropriate four-component framework.[107] The latter is subject of ongoing work in our laboratories.

The novel (e)amfX2C models are readily available for genuine two-component atomic and molecular SCF calculations including both HF and DFT. As these then often constitute the basis for more elaborate approaches such as (real-time) time-dependent *ansätze* as well as response-theory based approaches and post-HF electron-correlation

approaches in general, for example, configuration-interaction- or coupled-cluster-type wave-function expansions, our (e)amfX2C models are broadly applicable within a two-component quantum-chemical framework.

As a first demonstration of the capabilities of the (e)amfX2C models, we have applied them to the calculation of molecular spinor energies of representative closed and open-shell (super-)heavy homonuclear diatomic molecules of group 16 and 18, respectively, both within an HF and a DFT-based SCF *ansatz*. With these systems, namely Te_2 and Og_2, we have assessed the numerical accuracy of the (e)amfX2C Hamiltonian models by comparing to four-component reference data with respect to the ability to reproduce absolute spinor energies as well as relative energies defined as the atomic-like spin-orbit splittings of the inner-core shells. As a further test, we have calculated both the absolute contact density at the Cn nucleus and contact density shifts in copernicium fluoride compounds (CnF_n, $n = 2, 4, 6$) relative to the atomic value for the bare Cn atom. Finally, we have studied the performance of our (e)amfX2C Hamiltonian models for core-electron binding energies in the realm of X-ray spectroscopy by making use of an equation-of-motion coupled-cluster approach.

For the open- and closed-shell diatomic molecules we demonstrate that by applying our (e)amf PCE corrections to the X2C Hamiltonian models it is possible to match all corresponding four-component molecular spinor energies with μ-Hartree accuracy, *viz.* for inner- core to outer-valence electronic shells. This outstanding performance holds not only for two-component SCF calculations within a Kramers-restricted and Kramers-unrestricted HF *ansatz* but also within a DFT framework. Moreover, we show that scalar-relativistic two-electron PCE corrections are of utmost importance for a reliable description of core electronic shells within a two-component X2C Hamiltonian framework. The latter necessity manifests itself also in the calculation of absolute as well as relative contact densities at the Cn nucleus with respect to CnF_n ($n = 0, 2, 4, 6$) compounds, where their neglect can lead to sizeable discrepancies with respect to the same quantities obtained within a four-component framework. Although the (e)amf corrections are able to eliminate a substantial part of the scalar-relativistic and spin-orbit two-electron PCEs in the X2C framework, qualitative discrepancies between our two- and four-component results remain. We could trace the missing gap to the ^{4}DC reference data for the absolute contact density at the Cn nucleus in CnF_2 and, similarly, for the other CnF_n ($n > 2$) compounds, to originate from a contact density contribution of the Cn $1s$ shell whose contributions show a relative deviation of about 11% between two- and four-component data.

A comparison of X-ray core binding energies for At^-, $[AuCl_4]^{-1}$ and CnF_6 further highlights the significance of an appropriate account of two-electron PCE corrections in a two-component framework in order to unambiguously and systemically improvable approach ^{4}DC(G) results. In particular, we demonstrate that our (e)amfX2C models enable X2C calculations of X-ray ionisation potentials – and the accompanying resolution of fine-structure fingerprints of L- and M-edges in heavy- and superheavy-element complexes – where the transformation to two-components is performed *prior* to the (molecular) SCF step while yielding results both on par with corresponding *molecular* mean-field calculations and in excellent agreement with the parent four-component ones. Moreover, we illustrate that it is possible within our (e)amfX2C models to account for two-electron effects originating from the Gaunt interaction. To ultimately strive for genuine comparisons of computed X-ray spectroscopic data with experiment, an inclusion of the full Breit interaction, higher-order correlation effects as well as QED-corrections will be essential to establish a computational model of true predictive power.[89] While the former two factors are currently under consideration within the DIRAC developers community ,[108] QED corrections have very recently been put forward for correlated calculations in a two-component framework[109] and will be made available in a future extension of our (e)amfX2C models.

In summary, we are confident that the picture-change-error correction models for the X2C Hamiltonian presented in this contribution constitute an important milestone towards a universal and reliable applicability of relativistic two-component quantum chemical approaches maintaining the accuracy of the parent four-component one at a fraction of its computational cost. In order to corroborate the latter, we are currently undertaking comprehensive studies of zero-field splittings in p- and d-block molecules as well as the calculations of EPR parameters of d- and f-element complexes on the basis of our (e)amfX2C Hamiltonian models within a correlated computational framework. Finally, since relativistic real-time time-dependent DFT[110] and wave-function based correlated approaches such as the density matrix renormalization group model[111] provide access to the absorption spectra of complex molecular systems in the valence- or core-excited range including a variational account of spin-orbit interaction, we intend to apply these approaches within our (e)amfX2C framework to a set of representative molecular d-block and actinide compounds.

DEDICATION

We dedicate this work to the memory of the late Bernd Schimmelpfennig, who passed away unexpectedly in 2019. He was, among other contributions, a pioneer in making corrections for two-electron picture-change effects within a two-component Hamiltonian framework not only popular but also, for the first time, widely usable in quantum chemistry.

ACKNOWLEDGMENTS

SK thanks the SHC department at GSI Darmstadt for the support during his time at GSI. Part of the calculations were performed at the High-Performance Computing infrastructure provided by the GSI IT Department. MR acknowledges supports from the Research Council of Norway through a Centre of Excellence Grant (Grant No 252569) and a research grant (Grant No 315822), as well as computational resources provided by UNINETT Sigma2 – the National Infrastructure for High Performance Computing and Data Storage in Norway (Grant No. NN4654K). TS acknowledges funding from the European Research Council (ERC) under the European Union's Horizon 2020 research and innovation programme (grant agreement No 101019907).

AUTHOR'S CONTRIBUTIONS

All authors contributed equally to theory development. All programming and calculations were carried out by SK (DIRAC) and MR (ReSpect).

DATA AVAILABILITY

The data that support the findings of this study are openly available in ZENODO at https://doi.org/10.5281/zenodo.6414910, see also Ref. 112.

CONFLICTS OF INTEREST

The authors have no conflicts to disclose.

REFERENCES

[1]K. G. Dyall and K. Fægri, *Introduction to Relativistic Quantum Chemistry* (Oxford University Press, Oxford, 2007).
[2]M. Reiher and A. Wolf, *Relativistic Quantum Chemistry: The Fundamental Theory of Molecular Science* (Wiley-VCH, Weinheim, 2009).
[3]T. Saue, "Relativistic Hamiltonians for Chemistry: A Primer," ChemPhysChem **12**, 3077–3094 (2011).
[4]W. Liu, "Advances in Relativistic Molecular Quantum Mechanics," Phys. Rep. **537**, 59–89 (2014).
[5]T. Saue, R. Bast, A. S. P. Gomes, H. J. A. Jensen, L. Visscher, I. A. Aucar, R. Di Remigio, K. G. Dyall, E. Eliav, E. Fasshauer, T. Fleig, L. Halbert, E. D. Hedegård, B. Helmich-Paris, M. Iliaš, C. R. Jacob, S. Knecht, J. K. Laerdahl, M. L. Vidal, M. K. Nayak, M. Olejniczak, J. M. H. Olsen, M. Pernpointner, B. Senjean, A. Shee, A. Sunaga, and J. N. P. van Stralen, "The DIRAC Code for Relativistic Molecular Calculations," J. Chem. Phys. **152**, 204104 (2020).
[6]M. Repisky, S. Komorovsky, M. Kadek, L. Konecny, U. Ekström, E. Malkin, M. Kaupp, K. Ruud, O. L. Malkina, and V. G. Malkin, "ReSpect: Relativistic Spectroscopy DFT Program Package," J. Chem. Phys. **152**, 184101 (2020).
[7]T. Shiozaki, "BAGEL: Brilliantly Advanced General Electronic-Structure Library," WIREs Comput. Mol. Sci. **8**, e1331 (2018).
[8]Y. Zhang, B. Suo, Z. Wang, N. Zhang, Z. Li, Y. Lei, W. Zou, J. Gao, D. Peng, Z. Pu, Y. Xiao, Q. Sun, F. Wang, Y. Ma, X. Wang, Y. Guo, and W. Liu, "BDF: A Relativistic Electronic Structure Program Package," J. Chem. Phys. **152**, 064113 (2020).
[9]L. Belpassi, M. D. Santis, H. M. Quiney, F. Tarantelli, and L. Storchi, "BERTHA: Implementation of a Four-Component Dirac–Kohn–Sham Relativistic Framework," J. Chem. Phys. **152**, 164118 (2020).
[10]The generic acronym "X2C" for exact two-component Hamiltonians resulted from intensive discussions among H. J. Aa. Jensen, W. Kutzelnigg, W. Liu, T. Saue, and L. Visscher during the Twelfth International Conference on the Applications of Density Functional Theory DFT-2007, Amsterdam, 26–30 August 2007.
[11]M. Douglas and N. M. Kroll, "Quantum Electrodynamical Corrections to the Fine Structure of Helium," Ann. Phys. **82**, 89–155 (1974).
[12]B. A. Hess, "Relativistic Electronic-Structure Calculations Employing a Two-Component No-Pair Formalism with External-Field Projection Operators," Phys. Rev. A **33**, 3742–3748 (1986).
[13]C. Chang, M. Pelissier, and P. Durand, "Regular Two-Component Pauli-Like Effective Hamiltonians in Dirac Theory," Phys. Scr. **39**, 394 (1986).
[14]E. van Lenthe, E. J. Baerends, and J. G. Snijders, "Relativistic Regular Two-Component Hamiltonians," J. Chem. Phys. **99**, 4597 (1993).
[15]E. van Lenthe, J. G. Snijders, and E. J. Baerends, "The Zero-Order Regular Approximation for Relativistic Effects: The Effect of Spin-Orbit Coupling in Closed Shell Molecules," J. Chem. Phys. **105**, 6505 (1996).
[16]M. Barysz and A. J. Sadlej, "Infinite-Order Two-Component Theory for Relativistic Quantum Chemistry," J. Chem. Phys. **116**, 2696 (2002).
[17]M. Reiher and A. Wolf, "Exact Decoupling of the Dirac Hamiltonian. I.General Theory," J. Chem. Phys. **121**, 2037 (2004).
[18]M. Reiher and A. Wolf, "Exact Decoupling of the Dirac Hamiltonian. II. The Generalized Douglas-Kroll-Hess Transformation up to Arbitrary Order," J. Chem. Phys. **121**, 10945 (2004).

[19]M. Reiher, "Douglas–Kroll–Hess Theory: A Relativistic Electrons-Only Theory for Chemistry," Theor. Chem. Acc. **116**, 241–252 (2006).
[20]K. G. Dyall, "Interfacing Relativistic and Nonrelativistic Methods. I. Normalized Elimination of the Small Component in the Modified Dirac Equation," J. Chem. Phys. **106**, 9618 (1997).
[21]M. Filatov and D. Cremer, "Connection Between the Regular Approximation and the Normalized Elimination of the Small Component in Relativistic Quantum Theory," J. Chem. Phys. **122**, 064104 (2004).
[22]M. Filatov, "Comment on "Quasirelativistic Theory Equivalent to Fully Relativistic Theory" [J.Chem. Phys. 123, 241102 (2005)]," J. Chem. Phys. **125**, 107101 (2006).
[23]M. Filatov and K. G. Dyall, "On Convergence of the Normalized Elimination of the Small Component (NESC) Method," Theor. Chem. Acc. **117**, 333–338 (2007).
[24]H. J. A. Jensen and M. Iliaš, "BSS / DKH infinite order the easy way !" https://doi.org/10.6084/m9.figshare.12046158.v3 (2005), (Talk from REHE 2005).
[25]W. Kutzelnigg and W. Liu, "Quasirelativistic Theory Equivalent to Fully Relativistic Theory," J. Chem. Phys. **123**, 241102 (2005).
[26]W. Kutzelnigg and W. Liu, "Quasirelativistic Theory I. Theory in Terms of a Quasi-Relativistic Operator," Mol. Phys. **104**, 2225 (2006).
[27]W. Liu and D. Peng, "Infinite-Order Quasirelativistic Density Functional Method Based on the Exact Matrix Quasirelativistic Theory," J. Chem. Phys. **125**, 044102 (2006).
[28]M. Iliaš and T. Saue, "An Infinite-Order Two-Component Relativistic Hamiltonian by a Simple One-Step transformation," J. Chem. Phys. **126**, 064102 (2007).
[29]W. Liu and D. Peng, "Exact Two-Component Hamiltonians Revisited," J. Chem. Phys. **131**, 031104 (2009).
[30]L. Konecny, M. Kadek, S. Komorovsky, O. L. Malkina, K. Ruud, and M. Repisky, "Acceleration of Relativistic Electron Dynamics by Means of X2C Transformation: Application to the Calculation of Nonlinear Optical Properties," J. Chem. Theory Comput. **12**, 5823–5833 (2016).
[31]D. Peng and M. Reiher, "Exact Decoupling of the Relativistic Fock Operator," Theor. Chem. Acc. **131**, 1081–1100 (2012).
[32]J. Sikkema, L. Visscher, T. Saue, and M. Iliaš, "The Molecular Mean-Field Approach for Correlated Relativistic Calculations," J. Chem. Phys. **131**, 124116 (2009).
[33]K. G. Dyall, "An exact separation of the spin-free and spin-dependent terms of the Dirac-Coulomb-Breit Hamiltonian," J. Chem. Phys. **100**, 2118 (1994).
[34]J. Liu and L. Cheng, "An Atomic Mean-Field Spin-Orbit Approach within Exact Two-Component Theory for a Non-Perturbative Treatment of Spin-Orbit Coupling," J. Chem. Phys. **148**, 144108 (2018).
[35]M. Blume and R. E. Watson, "Theory of Spin-orbit Coupling in Atoms I. Derivation of the Spin-Orbit Coupling Constant," Proc. R. Soc. Lond. A **270**, 127–143 (1962).
[36]M. Blume and R. E. Watson, "Theory of Spin-Orbit Coupling in Atoms, II. Comparison of Theory with Experiment," Proc. R. Soc. Lond. A **271**, 565–578 (1963).
[37]B. A. Heß, C. M. Marian, U. Wahlgren, and O. Gropen, "A Mean-Field Spin-Orbit Method Applicable to Correlated Wavefunctions," Chem. Phys. Lett. **251**, 365 (1996).
[38]AMFI, an atomic mean-field spin-orbit integral program, 1996, Bernd Schimmelpfennig, University of Stockholm.
[39]I. F. Galván, M. Vacher, A. Alavi, C. Angeli, F. Aquilante, J. Autschbach, J. J. Bao, S. I. Bokarev, N. A. Bogdanov, R. K. Carlson, L. F. Chibotaru, J. Creutzberg, N. Dattani, M. G. Delcey, S. S. Dong, A. Dreuw, L. Freitag, L. M. Frutos, L. Gagliardi, F. Gendron, A. Giussani, L. González, G. Grell, M. Guo, C. E. Hoyer, M. Johansson, S. Keller, S. Knecht, G. Kovasevic, E. Källman, G. Li Manni, M. Lundberg, Y. Ma, S. Mai, J. P. Malhado, P. Å. Malmqvist, P. Marquetand, S. A. Mewes, J. Norell, M. Olivucci, M. Oppel, Q. M. Phung, K. Pierloot, F. Plasser, M. Reiher, A. M. Sand, I. Schapiro, P. Sharma, C. J. Stein, L. K. Sørensen, D. G. Truhlar, M. Ugandi, L. Ungur, A. Valentini, S. Vancoillie, V. Veryazov, O. Weser, T. A. Wesolowski, P.-O. Widmark, S. Wouters, A. Zech, J. P. Zobel, and R. Lindh, "OpenMolcas: From Source Code to Insight," J. Chem. Theory Comput. **15**, 5925–5964 (2019).
[40]K. Aidas, C. Angeli, K. L. Bak, V. Bakken, R. Bast, L. Boman, O. Christiansen, R. Cimiraglia, S. Coriani, P. Dahle, E. K. Dalskov, U. Ekström, T. Enevoldsen, J. J. Eriksen, P. Ettenhuber, B. Fernández, L. Ferrighi, H. Fliegl, L. Frediani, K. Hald, A. Halkier, C. Hättig, H. Heiberg, T. Helgaker, A. C. Hennum, H. Hettema, E. Hjertenæs, S. Høst, I.-M. Høyvik, M. F. Iozzi, B. Jansík, H. J. Aa. Jensen, D. Jonsson, P. Jørgensen, J. Kauczor, S. Kirpekar, T. Kjærgaard, W. Klopper, S. Knecht, R. Kobayashi, H. Koch, J. Kongsted, A. Krapp, K. Kristensen, A. Ligabue, O. B. Lutnæs, J. I. Melo, K. V. Mikkelsen, R. H. Myhre, C. Neiss, C. B. Nielsen, P. Norman, J. Olsen, J. M. H. Olsen, A. Osted, M. J. Packer, F. Pawlowski, T. B. Pedersen, P. F. Provasi, S. Reine, Z. Rinkevicius, T. A. Ruden, K. Ruud, V. V. Rybkin, P. Sałek, C. C. M. Samson, A. S. de Merás, T. Saue, S. P. A. Sauer, B. Schimmelpfennig, K. Sneskov, A. H. Steindal, K. O. Sylvester-Hvid, P. R. Taylor, A. M. Teale, E. I. Tellgren, D. P. Tew, A. J. Thorvaldsen, L. Thøgersen, O. Vahtras, M. A. Watson, D. J. D. Wilson, M. Ziolkowski, and H. Ågren, "The Dalton quantum chemistry program system," WIREs Comput. Mol. Sci. **4**, 269–284 (2014).
[41]C. v. Wüllen and C. Michauk, "Accurate and Efficient Treatment of Two-Electron Contributions in Quasirelativistic High-Order Douglas-Kroll Density-Functional Calculations," J. Chem. Phys. **123**, 204113 (2005).
[42]D. Peng, W. Liu, Y. Xiao, and L. Cheng, "Making Four- and Two-Component Relativistic Density Functional Methods Fully Equivalent Based on the Idea of "from Atoms to Molecule"," J. Chem. Phys. **127**, 104106 (2007).
[43]J. Autschbach, D. Peng, and M. Reiher, "Two-Component Relativistic Calculations of Electric-Field Gradients Using Exact Decoupling Methods: Spin-Orbit and Picture Change Effects," J. Chem. Theory Comput. **8**, 4239–4248 (2012).
[44]J. C. Boettger, "Approximate Two-Electron Spin-Orbit Coupling Term for Density-Functional-Theory DFT Calculations Using the Douglas-Kroll-Hess Transformation," Phys. Rev. B **62**, 7809–7815 (2000).
[45]A. J. Jenkins, H. Liu, J. M. Kasper, M. J. Frisch, and X. Li, "Variational Relativistic Complete Active Space Self-Consistent Field Method," J. Chem. Theory Comput. **15**, 2974–2982 (2019).
[46]L. N. Koulias, D. B. Williams-Young, D. R. Nascimento, A. E. DePrince, and X. Li, "Relativistic Time-Dependent Equation-of-Motion Coupled-Cluster," J. Chem. Theory Comput. **15**, 6617–6624 (2019).
[47]H. Hu, A. J. Jenkins, H. Liu, J. M. Kasper, M. J. Frisch, and X. Li, "Relativistic Two-Component Multireference Configuration Interaction Method with Tunable Correlation Space," J. Chem. Theory Comput. **16**, 2975–2984 (2020).
[48]M. Filatov, W. Zou, and D. Cremer, "Spin-orbit coupling calculations with the two-component normalized elimination of the small component method," J. Chem. Phys. **139**, 014106 (2013).

[49]W. Zou, M. Filatov, and D. Cremer, "Analytical energy gradient for the two-component normalized elimination of the small component method," J. Chem. Phys. **142**, 214106 (2015).
[50]J. Liu and L. Cheng, "Relativistic Coupled-Cluster and Equation-of-Motion Coupled-Cluster Methods," WIREs Comput. Mol. Sci. **11**, e1536 (2021).
[51]J. Netz, A. O. Mitrushchenkov, and A. Köhn, "On the Accuracy of Mean-Field Spin-Orbit Operators for 3d Transition-Metal Systems," J. Chem. Theory Comput. **17**, 5530 (2021).
[52]P. O. Löwdin, "On the Nonorthogonality Problem," Adv.Quant.Chem. **5**, 185 (1970).
[53]J. Thyssen, *Development and Applications of Methods for Correlated Relativistic Calculations of Molecular Properties*, Ph.D. thesis, University of Southern Denmark (2001).
[54]J. P. Perdew, R. G. Parr, M. Levy, and J. L. Balduz, "Density-Functional Theory for Fractional Particle Number: Derivative Discontinuities of the Energy," Phys. Rev. Lett. **49**, 1691–1694 (1982).
[55]J. P. Perdew and K. Schmidt, in *Density Functional Theory and Its Application to Materials*, edited by V. V. Doren, C. V. Alsenoy, and P. Geerlings (American Institute of Physics, Melville, 2001).
[56]J. P. Perdew, A. Ruzsinszky, J. Tao, V. N. Staroverov, G. E. Scuseria, and G. I. Csonka, "Prescription for the Design and Selection of Density Functional Approximations: More Constraint Satisfaction with Fewer Fits," J. Chem. Phys. **123**, 062201 (2005).
[57]Y. Ikabata and H. Nakai, "Picture–Change Correction in Relativistic Density Functional Theory," Phys. Chem. Chem. Phys. **23**, 15458–15474 (2021).
[58]S. Komorovsky, P. J. Cherry, and M. Repisky, "Four-Component Relativistic Time-Dependent Density-Functional Theory Using a Stable Noncollinear DFT Ansatz Applicable to Both Closed- and Open-Shell Systems," J. Chem. Phys. **151**, 184111 (2019).
[59]J. Kubler, K.-H. Hock, J. Sticht, and A. R. Williams, "Density Functional Theory of Non-Collinear Magnetism," J. Phys. F: Met. Phys. **18**, 469–483 (1988).
[60]L. M. Sandratskii, "Noncollinear Magnetism in Itinerant-Electron Systems: Theory and Applications," Adv. Phys. **47**, 91–160 (1998).
[61]C. van Wüllen, "Spin Densities in Two-component Relativistic Density Functional Calculations: Noncollinear Versus Collinear Approach," J. Comp. Chem. **23**, 779–785 (2002).
[62]G. Scalmani and M. J. Frisch, "A New Approach to Noncollinear Spin Density Functional Theory beyond the Local Density Approximation," J. Chem. Theory Comput. **8**, 2193–2196 (2012).
[63]J. H. Van Lenthe, R. Zwaans, H. J. J. Van Dam, and M. F. Guest, "Starting SCF Calculations by Superposition of Atomic Densities," J. Comp. Chem. **27**, 926–932 (2006).
[64]P. J. Mohr, B. N. Taylor, and D. B. Newell, "CODATA Recommended Values of the Fundamental Physical Constants: 2006," Rev. Mod. Phys. **80**, 633–730 (2008).
[65]K. G. Dyall, "Relativistic Double-Zeta, Triple-Zeta, and quadruple-Zeta Basis Sets for the Light Elements H–Ar," Theor. Chem. Acc. **135**, 128 (2016).
[66]K. G. Dyall, "Relativistic and Nonrelativistic Finite Nucleus Optimized Double Zeta Basis Sets for the 4p, 5p and 6p Elements," Theor. Chem. Acc. **99**, 366–371 (1998).
[67]K. G. Dyall, "Relativistic Quadruple-Zeta and Revised Triple-Zeta and Double-Zeta Basis Sets for the 4p, 5p, and 6p Elements," Theor. Chem. Acc. **115**, 441–447 (2006).
[68]K. G. Dyall, "Relativistic Double-Zeta, Triple-Zeta, and Quadruple-Zeta Basis Sets for the 7p Elements, with Atomic and Molecular applications," Theor. Chem. Acc. **131**, 1172 (2012).
[69]K. G. Dyall, "Relativistic Double-Zeta, Triple-Zeta, and Quadruple-Zeta Basis sets for the 5d elements Hf–Hg," Theor. Chem. Acc. **112**, 403–409 (2004).
[70]K. G. Dyall and A. S. P. Gomes, "Revised Relativistic Basis Sets for the 5d Elements Hf–Hg," Theor. Chem. Acc. **125**, 97–100 (2009).
[71]K. G. Dyall, "Relativistic Double-Zeta, Triple-Zeta, and Quadruple-Zeta Basis Sets for the 6d Elements Rf–Cn," Theor. Chem. Acc. **129**, 603–613 (2011).
[72]Available from the Dirac web site, `http://dirac.chem.sdu.dk`.
[73]R. Lindh, P.-A. Malmqvist, and L. Gagliardi, "Molecular Integrals by Numerical Quadrature. I. Radial Integration," Theor. Chem. Acc. **106**, 178–187 (2001).
[74]V. Lebedev, "Values of the Nodes and Weights of Ninth to Seventeenth Order Gauss-Markov Quadrature Formulae Invariant under the Octahedron Group with Inversion," Zh. Vychisl. Mat. Mat. Fiz. **15**, 48–54 (1975).
[75]V. Lebedev, "Quadratures on a Sphere," Zh. Vychisl. Mat. Mat. Fiz. **16**, 293–306 (1976).
[76]V. I. Lebedev, "Spherical Quadrature Formulas Exact to Orders 25-29," Sibirsk. Mat. Zh. **18**, 132–142 (1977).
[77]P. Pulay, "Convergence acceleration of iterative sequences. the case of scf iteration," Chemical Physics Letters **73**, 393–398 (1980).
[78]J. P. Perdew, K. Burke, and M. Ernzerhof, "Generalized Gradient Approximation Made Simple," Phys. Rev. Lett. **77**, 3865–3868 (1996).
[79]J. P. Perdew, M. Ernzerhof, and K. Burke, "Rationale for Mixing Exact Exchange with Density Functional Approximations," J. Chem. Phys. **105**, 9982–9985 (1996).
[80]C. Adamo and V. Barone, "Toward Chemical Accuracy in the Computation of NMR Shieldings: the PBE0 Model," Chem. Phys. Lett. **298**, 113–119 (1998).
[81]J. F. Ogilvie and Y. Wang, "Potential-Energy Functions of Diatomic Molecules of the Noble Gases I. Like Nuclear Species," J. Mol. Struct. **273**, 277–290 (1992).
[82]A. Shee, S. Knecht, and T. Saue, "A Theoretical Benchmark Study of the spectroscopic Constants of the Very Heavy Rare Gas Dimers," Phys. Chem. Chem. Phys. **17**, 10978 (2015).
[83]J.-B. Rota, S. Knecht, T. Fleig, D. Ganyushin, T. Saue, F. Neese, and H. Bolvin, "Zero Field Splitting of the Chalcogen Diatomics using Relativistic Correlated Wave-Function Methods," J. Chem. Phys. **135**, 114106 (2011).
[84]L. Trombach, S. Ehlert, S. Grimme, P. Schwerdtfeger, and J.-M. Mewes, "Exploring the Chemical Nature of Super-Heavy Main-Group Elements by means of Efficient Plane-Wave Density-Functional Theory," Phys. Chem. Chem. Phys. **21**, 18048–18058 (2019).
[85]S. Hu and W. Zou, "Stable Copernicium Hexafluoride (CnF_6) with an Oxidation State of +VI," Phys. Chem. Chem. Phys. **24**, 321 (2022).
[86]S. Knecht, S. Fux, R. van Meer, L. Visscher, M. Reiher, and T. Saue, "Mössbauer Spectroscopy for Heavy Elements: A Relativistic Benchmark Study of Mercury," Theor. Chem. Acc. **129**, 631–650 (2011).
[87]S. Knecht and T. Saue, "Nuclear Size Effects in Rotational Spectra: A Tale with a Twist," Chem. Phys. **401**, 103–112 (2012).

[88]A. Shee, T. Saue, L. Visscher, and A. S. P. Gomes, "Equation-of-Motion Coupled-Cluster Theory Based on the 4-Component Dirac-Coulomb(-Gaunt) Hamiltonian. Energies for Single Electron Detachment, Attachment, and Electronically Excited States," J. Chem. Phys. **149** (2018), 10.1063/1.5053846.
[89]L. Halbert, M. L. Vidal, A. Shee, S. Coriani, and A. Severo Pereira Gomes, "Relativistic EOM-CCSD for Core-Excited and Core-Ionized State Energies Based on the Four-Component Dirac–Coulomb(-Gaunt) Hamiltonian," J. Chem. Theory Comput. **17**, 3583–3598 (2021).
[90]M. Hargittai, A. Schulz, B. Réffy, and M. Kolonits, "Molecular Structure, Bonding, and Jahn-Teller Effect in Gold Chlorides: Quantum Chemical Study of $AuCl_3$, Au_2Cl_6, $AuCl_4^-$, AuCl, and Au_2Cl_2 and Electron Diffraction Study of Au_2Cl_6," J. Am. Chem. Soc. **123**, 1449–1458 (2001).
[91]M. A. Ambroise, A. Dreuw, and F. Jensen, "Probing Basis Set Requirements for Calculating Core Ionization and Core Excitation Spectra Using Correlated Wave Function Methods," J. Chem. Theory Comput. **17**, 2832–2842 (2021).
[92]L. Visscher and T. Saue, "Approximate Relativistic Electronic Structure Methods based on the Quaternion Modified Dirac Equation," J. Chem. Phys. **113**, 3996–4002 (2000).
[93]T. Saue, *Principles and Applications of Relativistic Molecular Calculations*, Ph.D. thesis, University of Oslo (1996).
[94]C. Pellegrini, A. Marinelli, and S. Reiche, "The Physics of X-Ray Free-Electron Lasers," Rev. Mod. Phys. **88**, 015006 (2016).
[95]An overview on X-ray free-electron laser facilities can be found at: `https://www.xfel.eu/facility/comparison/index_eng.html`.
[96]F. Lin, Y. Liu, X. Yu, L. Cheng, A. Singer, O. G. Shpyrko, H. L. Xin, N. Tamura, C. Tian, T.-C. Weng, X.-Q. Yang, Y. S. Meng, D. Nordlund, W. Yang, and M. M. Doeff, "Synchrotron X-Ray Analytical Techniques for Studying Materials Electrochemistry in Rechargeable Batteries," Chem. Rev. **117**, 13123–13186 (2017).
[97]M. Chergui and E. Collet, "Photoinduced Structural Dynamics of Molecular Systems Mapped by Time-Resolved X-ray Methods," Chem. Rev. **117**, 11025–11065 (2017).
[98]P. M. Kraus, M. Zürch, S. K. Cushing, D. M. Neumark, and S. R. Leone, "The Ultrafast X-Ray Spectroscopic Revolution in Chemical Dynamics," Nat. Rev. Chem. **2**, 82–94 (2018).
[99]P. Norman and A. Dreuw, "Simulating X-Ray Spectroscopies and Calculating Core-Excited States of Molecules," Chem. Rev. **118**, 7208–7248 (2018).
[100]K. O. Kvashnina and S. M. Butorin, "High-Energy Resolution X-Ray Spectroscopy at Actinide $M_{4,5}$ and Ligand K Edges: What We Know, What We Want to Know, and What We Can Know," Chem. Comm. **58**, 327–342 (2021).
[101]M. Kadek, L. Konecny, B. Gao, M. Repisky, and K. Ruud, "X-ray Absorption Resonances Near $L_{2,3}$-Edges from Real-Time Propagation of the Dirac–Kohn–Sham Density Matrix," Phys. Chem. Chem. Phys. **17**, 22566–22570 (2015).
[102]C. South, A. Shee, D. Mukherjee, A. K. Wilson, and T. Saue, "4-Component Relativistic Calculations of L3 Ionization and Excitations for the Isoelectronic Species UO_2^{2+} OUN^+ and UN_2," Phys. Chem. Chem. Phys. **18**, 21010 (2016).
[103]T. F. Stetina, J. M. Kasper, and X. Li, "Modeling $L_{2,3}$-Edge X-Ray Absorption Spectroscopy with Linear Response Exact Two-Component Relativistic Time-Dependent Density Functional Theory," J. Chem. Phys. **150**, 234103 (2019).
[104]L. Konecny, J. Vicha, S. Komorovsky, K. Ruud, and M. Repisky, "Accurate X-ray Absorption Spectra near L- and M-edges from Relativistic Four-Component Damped Response Time-Dependent Density Functional Theory," Inorg. Chem.. **61**, 830–846 (2022).
[105]C. Puzzarini, J. Bloino, N. Tasinato, and V. Barone, "Accuracy and Interpretability: The Devil and the Holy Grail. New Routes across Old Boundaries in Computational Spectroscopy," Chem. Rev. **119**, 8131–8191 (2019).
[106]The scalar relativistic atomic SCF code RELSCF is based on an atomic SCF code written by Enrico Clementi [*Ab initio computations in atoms and molecules*, IBM Journal Res. and Develop. **9**, 2–19, (1965)] and scalar relativity was introduced by Bernd Hess.
[107]M. Kadek, M. Repisky, and K. Ruud, "All-Electron Fully Relativistic Kohn-Sham Theory for Solids Based on the Dirac-Coulomb Hamiltonian and Gaussian-Type Functions," Phys. Rev. B **99**, 205103 (2019).
[108](2021), Private communications, DIRAC developers meeting 2021, online, Sep 2nd,.
[109]A. Sunaga and T. Saue, "Towards Highly Accurate Calculations of Parity Violation in Chiral Molecules: Relativistic Coupled-Cluster Theory Including QED-Effects," Mol. Phys. **119**, e1974592 (2021).
[110]M. Repisky, L. Konecny, M. Kadek, S. Komorovsky, O. L. Malkin, V. G. Malkin, and K. Ruud, "Excitation Energies from Real-Time Propagation of the Four-Component Dirac-Kohn-Sham Equation," J. Chem. Theory Comput. **11**, 980–991 (2015).
[111]Alberto Baiardi, private communication, March 2022.
[112]S. Knecht, M. Repisky, H. J. Aa. Jensen, and T. Saue, "Replication Data for: Exact Two-Component Hamiltonians for Relativistic Quantum Chemistry: Two-Electron Picture-Change Corrections Made Simple," ZENODO (2022), 10.5281/zenodo.6414910.